FTIR spectroscopy of nanodiamonds: Methods and Interpretation

Tristan Petit, Ljiljana Puskar

Institute of Methods for Materials Development, Helmholtz Zentrum Berlin für Materialien und Energie GmbH, Albert-Einstein-Strasse 15, 12489 Berlin, Germany

Email: tristan.petit@helmholtz-berlin.de, ljiljana.puskar@helmholtz-berlin.de

Keywords: FTIR, nanodiamonds, surface chemistry, *in situ* spectroscopy, ATR, DRIFT

Abstract

Fourier transform infrared spectroscopy (FTIR) is highly sensitive to the surface chemistry of nanodiamonds. In this review, we discuss the different FTIR methods available to characterize nanodiamonds and highlight their advantages and limitations. We also summarize the possible assignments of FTIR spectra of nanodiamonds reported in the literature and discuss FTIR spectra of nanodiamonds modified by different surface treatments. Current work of FTIR applied to *in situ* and *operando* characterization of nanodiamonds, in particular nanodiamonds exposed to water or characterized during electrochemical and photocatalytic processes, are also discussed. Finally, perspectives regarding possible future FTIR development for nanodiamonds characterization are proposed.

1. Introduction

One of the key features of nanodiamonds (NDs), as compared to many other nanoparticles, is their rich surface chemistry that can open wide possibilities for functionalization or fine-tuning of their chemical and electronic properties. In addition to the stability, biocompatibility and fluorescence properties of the diamond core, surface properties of NDs have enabled the development of medical, tribology, catalytic or sensing applications.[1–3] To this aim, the reliable characterization of NDs surface chemistry is essential.

Fourier Transform Infrared (FTIR) spectroscopy has been employed extensively for the characterization of NDs over the last 20 years. The high sensitivity of FTIR to the surface functional groups of NDs, its non-destructive nature and generally easy sample preparation have contributed to establish FTIR as a reference method for the characterization of NDs surface chemistry. The versatility of FTIR in terms of experimental schemes applied to nanoparticles makes FTIR a method of choice for measurements from routine control of surface functionalization to advanced *operando* measurement of complex chemical processes. Some of the work on the characterisation of nanoparticles, their surface reactions and application to catalysis reactions using different modes of infrared spectroscopy has been highlighted in recent reviews.[4–6]

Interpretation of FTIR spectra is however not an easy task because the high sensitivity of FTIR to chemical environment imply that FTIR spectra is also very sensitive to experimental conditions (sample preparation, atmosphere...). Contrary to electron and X-ray spectroscopies, FTIR is not element-specific and different chemical bonds may have IR-active vibrational modes at the same frequencies.

Unambiguous interpretation of FTIR spectra often requires the use of complementary characterization techniques. On the other hand, FTIR does not necessitate vacuum conditions and is therefore well adapted for *operando* measurements in liquid or gaseous environments.

FTIR spectra of NDs can vary significantly between two studies, depending on the type of NDs, their surface treatments and environmental conditions. Indeed, NDs may refer to different type of materials and prior knowledge on the production method and processing steps are generally required to analyse FTIR spectra. NDs can be produced by various synthesis methods, the most common ones being detonation synthesis and milling of synthetic diamond films grown by High Pressure High Temperature (HPHT).[7] Detonation NDs (DNDs) have a size range of 3-6 nm, a defective structure and a wide variety of functional groups after synthesis.[1,7] The cleaning processes vary between providers and materials labelled as DNDs may have very different surface chemistries or purity and hence different FTIR signatures. Extensive research towards the homogenization of the surface of DNDs has therefore been conducted.[8] On the other hand, HPHT NDs consist of well-faceted crystallites with less defects and larger sizes as compared to DNDs. Size and structural properties of NDs affect FTIR spectra therefore similar surface treatments performed on NDs from different sources may lead to different FTIR signatures. Vibrational frequencies from functional groups on NDs surface and similar groups on organic molecules or bulk diamond often differ, therefore direct comparison with literature from other carbon-based materials should be done with care.

In this review, we present the various FTIR methods used thus far for the characterisation of NDs. The advantages and drawbacks of each methods will be discussed, and particularities associated with their applications to nanoparticles will be highlighted. Then, an overview of possible assignments of FTIR spectral features on NDs will be provided. Examples of FTIR spectra after surface treatments, usually applied to homogenize the NDs surface before further functionalization, will be discussed. We intentionally restrain this review to the functionalization of NDs surface with simple functional groups but examples of FTIR spectra of NDs with more complex functionalization are available in the references [9–21]. Finally, we discuss further directions for *in situ* FTIR measurements *i.e.* in conditions relevant to real applications, and for *operando* measurements, *i.e.* during chemical reactions relevant to real applications. *In situ* conditions could refer to aqueous environment with redox species for electrochemical applications or inside living cells for biomedical applications, while *operando* would mean under potential in aqueous environment for electrochemical reactions or at high temperature with reactants for heterogeneous catalysis for example. To our opinion, *in situ* and *operando* FTIR could strongly benefit the NDs community for the development of new applications in nanomedicine, catalysis or energy conversion and storage.

2. FTIR spectroscopy

Infrared absorption spectroscopy is a well-established vibrational technique used for chemical characterisation of material at the molecular level. In the infrared active transitions the electric dipole moments of vibrating functional groups undergo change as they interact with (absorb) the incoming infrared light. Absorptions of IR radiation by different functional groups within the sample are plotted as a function of wavelength, typically presented in units of wavenumbers or cm^{-1}.

The theory and basic principles of infrared spectroscopy are extensively covered and reviewed in the literature and will not be discussed here.[22–25] Comprehensive database of vibrational frequencies is readily available. Infrared spectrometers are routinely used in analytical laboratories, particularly since the introduction of FTIR spectrometers in 1950s where the combination of a Michelson

Interferometer and Fourier transformation enabled superior data quality and acquisition speed.[24] The so called Cones advantage of FTIR provides measurements with high accuracy and high spectral resolution, Jacquinot or high throughput advantage enables data of higher Signal-to-Noise ratio, whereas Fellget or multiplex advantage ensures that all the frequencies from the infrared source are detected simultaneously.[22,24] In addition, FTIR spectrometers are capable of recording spectra very rapidly by running the spectrometer in the rapid or step scan collection modes for which a time resolution of 40 ms or several hundreds of nanoseconds respectively can be achieved for a spectrum of 4 cm^{-1} spectral resolution. This is taken advantage of when monitoring time dependent processes.[26]

A Michelson interferometer consists of a beam splitter and two reflecting mirrors one of which is movable over the range of distances. A light from a broadband infrared source (global source such as metal wire, Nernst bar or synchrotron source) is collimated and directed onto a beam splitter (partially reflective mirror) that splits the beam into two portions. The partial beams reflected off the mirror surfaces are recombined back at the beamsplitter with a position dependent phase shift due to the path length difference that they had travelled. The beam leaving the interferometer is focused on the sample and then detected by a detector. The interferogram, measured as an intensity of the combined IR beams as a function of the moving mirror displacement is converted to a spectrum by a Fourier Transformation.[27] Commercially available instruments are highly adaptable to different measurement modes and spectral regions which, together with the suitable sample preparation method and data treatment, can provide the information on almost any sample type.

Overview of the FTIR methods most commonly utilised for the characterisation of NDs will be given next, however some other potential and emerging FTIR techniques that could become suitable for NDs will be highlighted later in the perspectives. Figure 1 shows the schematic of the three most widely used methods in the current literature on NDs. An option of flow through of gas and/or liquid and sample illumination to allow for *in situ* measurements are also shown. Most of the work covers the Mid-Infrared spectral region (MIR), although some studies on meteoritic NDs in the Far-Infrared (FIR) region were also reported.[28,29] Spectral resolution was typically held between 4 and 8 cm^{-1}.

2.1. Transmission Methods

Transmission measurements rely on the absorption of IR radiation as it passes through the sample. Transmittance depends on the sample thickness with the attenuation of transmitted light following the Beer-Lambert law.[22] This is the most commonly used method for the characterization of NDs. Two different sample preparation methods are described.

2.1.1. Sample material pressed as pellets in IR transparent matrix

In this method, a mixture of dry NDs in potassium bromide (KBr) matrix is pressed into thin pellets. The IR beam passes through the pellets placed inside the sample compartment of a FTIR spectrometer before being detected by a detector. The pellets can further be placed inside an environmental sample chamber that has IR transparent windows on each side to let the beam through. This allows for the changes of environmental conditions such as for example the temperature control or introduction of a gas flow for monitoring of *in situ* reactions (Figure 1a). This measurement approach was used primarily for the investigation of functional groups on NDs that underwent different treatments and surface modifications, but also adsorption of water on NDs surfaces by controlled exposure to different relative humidity conditions.

The pellet thickness and the sample concentration should be optimized to preserve the linearity of Beer-Lambert law and the sample material should be sufficiently transparent (absorbance <1). For NDs, the pellets can be prepared from several mg of sample mixed with ~140 mg of KBr and pressed under 0.9 MPa for a 13 mm diameter pellet.[30] The spectra are measured through the pellet, either under ambient conditions or in an evacuated sample chamber to minimize water vapor influence. Pure KBr pellets (kept or pretreated under the same conditions as the pellets containing the sample) are used for background measurement subtraction also accounting for any water adsorbed by KBr. AgCl is sometimes used as a matrix material but mainly to evaluate KBr and identify any potential interaction and influence it may have on the sample spectra.[30,31]

For the quantitative analysis using NDs pressed in pellets, ensuring a constant concentrations and sample thickness between different measurements may be difficult. Furthermore, the drying of the KBr pellet requires a significant amount of time since KBr is hygroscopic. Spectral distortions may also appear in the transmission spectra of powdered samples pressed in pellets.[32] The so-called Christiansen effect appears as an anomalous transmittance at wavelengths at which the refractive index of the sample and the matrix are equal.[33]

2.1.2.Thin films on an IR transparent substrate

Nanomaterial films can directly be placed on an infrared transparent substrate by drop casting or spin coating. Single crystalline silicon substrate materials are most commonly used as the material is transparent in the infrared region down to around 1500 cm^{-1}.[34–36] Although mainly used for qualitative structural information of the bulk material, some information from the layer structures and the density of IR active structural groups were reported in literature.[34] The advantage of this approach is that it is compatible with ultrahigh vacuum (UHV) conditions and NDs can be characterized directly after harsh treatments such as hydrogen plasma without air exposure, which cannot be done with KBr pellets.[35,37] Disadvantages are the IR cut off due to the substrate material and the possible appearance of interference effects in the thin film which can induce large errors in the quantitative analysis of spectra.[34]

This method was reported in identification of surface functionalities on diamonds of different origins, [37] influence of different NDs treatments,[35] as well as pH dependence measured on dried NDs on silicon substrate at ambient conditions.[36] Background measurement are taken through the clean substrate.

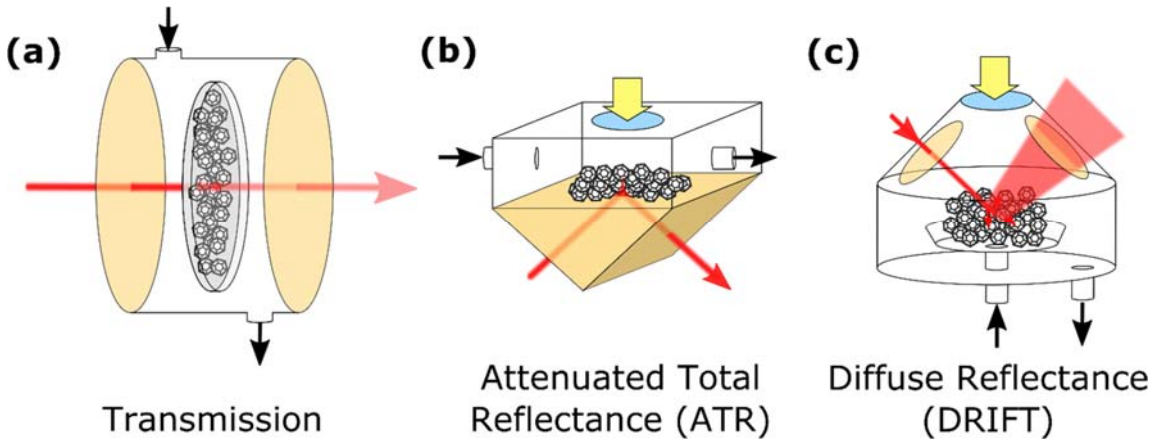

Figure 1: Schematic representation of transmission FTIR (a), ATR FTIR (b) and DRIFT (c) measurements for the characterization of NDs. These methods can be applied on dry NDs but also during exposure to various atmospheric conditions (in situ) or during electro/photochemical and catalytic processes (operando). IR and UV/Vis transparent materials are highlighted in orange and blue, respectively. Red and yellow arrows are highlighting beam path for IR and UV/Vis light. Black arrows illustrate inlets and outlets for gas or liquid exposures.

2.2. Reflectance Methods

In a reflectance measurement the infrared radiation beam interacts with the surface material and is reflected from an interface where a change of refractive index occurs. It can be internal reflectance such as in attenuated total reflectance (ATR) mode, or external reflectance. For highly reflective materials with polished surfaces the external reflectance at near normal incidence is used. Kramers-Kronig transformation describes the reflected absorbance in terms of the absorption index and refractive index spectra. For the powdered samples, the diffuse reflectance component is more significant and the Kramers-Kronig transformation is not sufficient. External reflectance from very thin layers is measured in grazing incidence mode and the reflectance intensity is dependent on the polarization of incidence radiation. [23]

2.2.1. Attenuated Total Reflectance (ATR)

ATR FTIR spectroscopy is based on a total internal reflection of IR light from an interface between two mediums of different optical density.[38] In such a setup, NDs are deposited on an IR transparent material of high refractive index (optical density) such as Ge, ZnSe, Si or diamond as the most commonly used ones (Figure 1b). The infrared light passing through the internal reflection element (ATR crystal) at angles above the critical angle undergoes total internal reflection which produces an evanescent wave propagating through the sample. The absorbance is measured from the sample volume penetrated by this exponentially decaying evanescent wave, which thickness is generally described by the depth of penetration d_p:

$$d_p = \frac{\lambda}{2\pi n_1 \sqrt{sin^2\,\theta - \left(\frac{n_2}{n_1}\right)^2}}$$

The distance that the light penetrates into the sample is dependent on the wavelength of the light (λ), the angle of incidence θ and refractive index of both the ATR element (n_1) and the sample (n_2). For ATR measurements, the absorbance is therefore not dependent on the sample thickness like in a transmission measurement. This is of particular advantage for investigation of reactions at the interface of NDs with highly absorbing liquids such as water. Due to the short effective path length, the solution contribution beyond the interfacial region is small.[5] For the MIR region the penetration depths are usually less than 5 microns, although the actual signal is collected from 2-3 times that distance.[39] The high refractive index of an ATR crystal also focuses the beam and improves the spatial resolution on the sample which has been utilised in the ATR imaging, however one should note that

the special resolution is of several micrometers in size for the MIR region.[39] Different ATR accessories exist with single or multiple reflections. The crystal material can be optimised for the spectral region of interest (e.g. lower energy cut off) and the sample environment (e.g. pH) but also the depth of penetration.[40] ZnSe, Si or diamond crystals are mostly used but hybrid structures, such as diamond-coated Si crystal, have also been applied to NDs.[41] In addition, the depth of penetration can be varied by changing the angle of incidence allowing for depth profiling.[42] The wavelength dependency of d_p in eq. (1) should be taken into consideration in the quantitative investigations and when comparing to transmission measurements as the absorbance peaks at higher wavelengths are enhanced. Although not widely reported in the study of nanomaterials, FIR region can be used with suitable choice of ATR material (e.g. diamond) and the focusing elements.[43]

Apart from the band intensity variation, the distortion of band shapes and shifts towards lower frequencies affect the ATR spectra as compared to transmission measurements.[44] This happens for strongly absorbing bands due to the anomalous dispersion of the sample refractive index, like in the case of water.[44] Advanced ATR correction algorithms are available that mostly remove these distortions.[45]

Sample preparation generally consists of drop casting a suspension of NDs in aqueous solution (microliter range) onto an ATR crystal and drying it off to produce a thin film. Such film is a multilayer of NDs, estimated by optical microscopy to have over 10 µm thickness for 1 µL of NDs suspension (1.5 µg NDs to 1 mL water).[46] The sample has to be in very good contact with the ATR crystal as any small gaps would affect and decrease the absorbance. Background reference is taken from the blank ATR crystal, mounted inside the sample compartment of a FTIR spectrometer which can either be purged with dry air or evacuated to remove gas phase water absorption bands. Investigation of different surface functionalities on NDs is done by referencing the dry film (purged with N_2 or inert gas) against the clean ATR crystal.[47] ATR FTIR spectra can also be obtained directly from NDs by pressing a diamond crystal of an ATR accessory against the sample. NDs of different size distribution (4-50 nm), synthetic preparation methods and their fluorinated derivatives were investigated using this method.[48] Water interaction with surface modified NDs exposed to ambient air for different times after the surface treatment were also studied using this sampling method.[49]

To investigate the interaction of solvent molecules with NDs surface *in situ*, the solvent molecules (e.g. H_2O[47], EtOH[46]) are introduced into a flow through sample chamber positioned above the ATR crystal, by flowing gas molecules over the dry NDs layer. To measure the interactions of NDs in liquid solutions, the difference spectra are generally calculated. Here the spectra of NDs exposed to a liquid solution (matrix solution containing the solute of interest) is subtracted from the background spectra measured from the NDs exposed to the matrix aqueous solution alone.[50] ATR FTIR was used to study the dynamics of the adsorption and conformational changes of the proteins on NDs.[51] *In situ* light illumination is also possible and has been for example applied on TiO_2 nanoparticles.[52]

2.2.2. Diffuse reflectance infrared Fourier transform (DRIFT)

This technique is suitable for powdered samples and samples sensitive to preparation methods such as pellets pressing. The powders are placed in a sample container either pure or diluted in KBr or KCl. Infrared radiation illuminating the sample is reflected from the surface of nanoparticles but some portion is absorbed or scattered from the NDs (Figure 1c). The diffused reflection is generally weak and is collected by ellipsoidal or parabolic mirrors. Sample chambers fitted with KBr windows and options for the environmental conditions change (temperature, pressure, gas flow, light illumination) allow for the *in situ* measurements.

The reproducibility of DRIFT signal intensities could be problematic as it is sensitive to nanoparticle size, compactness and distribution within the sample container. The nanoparticle size distribution of both the sample and the calibration standard should be minimized for better comparison between different measurements. Absorbance, reflectivity and refractive index of the sample material all play an important role and complex models for quantification of signal intensities are required to account for different contribution of each.[53–55]

DRIFT measurements are extensively used on nanoparticle surfaces with a range of adsorbed molecules and *in situ* monitoring of reactions with gaseous and adsorbed species[56–58] or to study solid oxide catalysis under operating conditions.[59] Some reports have demonstrated that this method can be applied to NDs as discussed in section 5.3.[60–62]

2.2.3.Grazing angle reflectance (GAR)

GAR is typically used for characterization of very thin films. It was applied to HPHT NDs to investigate size and evolution of surface functional groups down to 1 nm in size.[63] A small drop (~100 µL) of NDs solution is casted onto the Au reflective mirrors to produce thin layers. Au mirrors were made hydrophilic by oxidizing them in radio-frequency plasma to ensure good adhesion of NDs.

In this configuration the reflectance intensity is dependent on the polarization of the incident radiation and the angle of incidence (up to a maximum at 87°). Only the vibrational modes with a dipole moment perpendicular to the surface are infrared active (surface selection rule applies) and therefore the intensity of IR bands measured by GAR could differ from the transmission measurements. GAR measurements of thin films on metallic surfaces have also been used to study the molecular orientation and average conformation order.[23] Growing nanostructured diamond layers over metallic films has also been shown to dramatically enhance the sensitivity of GAR FTIR.[64]

2.3. Photoacoustic FTIR studies (PAS FTIR)

PAS is a noninvasive and sample preparation free FTIR absorbance technique, suitable for a wide range of samples including highly absorbing ones. The energy absorbed by the sample produces heat that is transferred from the sample into the surrounding He gas and the temperature oscillations are detected by a microphone. The penetration depth of the infrared light can be varied by changing the modulation frequencies induced by the interferometer mirror scanning speed providing the best depth resolution available by IR sampling techniques.[22] The signal intensity is linearly related to sample concentration, absorptivity and sampling depth. Carbon black is generally used as background correction to account for any variations in the source power density or amplifier electronics.[65]

Ando et al. reported improved surface sensitivity of PAS in the analysis of chemisorbed hydrogen and oxygen on the surface of diamond powders as compared to diffuse reflectance and transmission method using KBr pellets.[66] Advantage of PAS in the measurements of powders is the absence of dispersion effects.[32,67] Potential disadvantage for powder samples is in the reproducibility of the peak intensities.[66]

3. Interpretation of FTIR spectra of nanodiamonds

In this section, an overview of attributions of the various FTIR features on NDs is provided. They are classified by the main categories of bands typically observed on NDs and by increasing absorbance frequency. We focus here on the MIR range (900-4000 cm^{-1}), which is widely documented in the literature. All the features discussed in the text are summarized in Table 1. Although not all the bands reported in the literature are mentioned here, the most important contributions are included. For each assignment, the type of NDs as well as the FTIR method used for the characterization are highlighted.

3.1. "Fingerprint" region (900-1500 cm^{-1})

This IR region is notoriously difficult to interpret on NDs because many contributions from the diamond core and surface groups are overlapping. Diamond core features are mainly related to C-C lattice vibrations and various types of defects. The diamond lattice vibration at 1332 cm^{-1} corresponds to the first order Raman band and is typically not detected by FTIR. However, this band was clearly visible in several studies and its appearance was interpreted to be the result of broken symmetry of the diamond C-C bond near the surface due to the surface groups.[68] In the H-terminated or F-terminated NDs in particular, the diamond lattice vibration is better resolved due to its smaller overlap with C-H and C-F bonds.[13,48,68–71] This vibrational mode may be screened by oxygen-related surface groups on other types of NDs.

Nitrogen-induced defects may appear with different contributions in the spectra, especially as detonation NDs have large amount of nitrogen in the core but also a highly defective structure compared to bulk diamond. A broad feature in the 1100-1500 cm^{-1} region is typically assigned to nitrogen impurities [29,31,68] with some more defined vibrational modes from nitrogen-based defects reported at 1180, 1260 and 1360 cm^{-1}.[29]

Surface groups are contributing significantly to the IR fingerprint region. The main contribution from oxygen-related groups is usually ascribed to C-O-C bending modes of ether-like groups, lactones or acid anhydrides around 1100-1140 cm^{-1},[31,68,69,72] however C-O stretching modes of hydroxyl groups are also detected in this region.[31,73] C-O bending modes of epoxy structure or ether group are reported at 1260 cm^{-1},[10,31,73,74] and acid anhydride-related vibrations at 940, 1290 and 1370 cm^{-1} on oxidized HPHT NDs.[75] C-N stretching and amide III bands also contribute to the 1210-1320 cm^{-1} region for NDs having high nitrogen content or aminated surface.[61,76,77] Finally, C-H bending modes around 1460 cm^{-1} are observed when hydrogenated groups are present on the NDs surface.[36,47,49,50,69,70,74]

3.2. Amide bands (1500-1665 cm^{-1})

Amide bands were rarely reported on pristine NDs,[69] because in detonation NDs most of nitrogen atoms are incorporated in the core with little influence on the surface chemistry.[78] However for the case of aminated NDs, amide I and II bands related to C=O and C-N stretching and N-H bending modes, have been reported.[69,77,79] Care has to be taken as these bands are often difficult to differentiate from OH bending mode from water and NDs hydroxyl groups. Additional bands related to C=N stretching (1610 cm^{-1}) and N-H scissor (1514 cm^{-1}) were reported on aminated diamond powder.[80]

3.3. C=C stretching modes (1535-1595 cm^{-1})

Several studies have tentatively attributed bands in the range of 1535-1595 cm^{-1} to C=C stretching modes.[19,50,61,63,73,81,82] Although this band should not be IR active, it has been proposed that

polarization from nearby oxygen atoms could lead to appearance of this band.[72,74] In FTIR measurements at ambient conditions, in some special cases overlap with OH bending vibrations from water should however also be considered.

3.4. OH bending modes (1540-1650 cm^{-1})

The OH bending modes of hydroxyl groups on diamond at 1620-1630 cm^{-1} are not easily distinguished from those from water molecules when measured at ambient conditions.[10,74,76,83] Measurement under vacuum enables desorption of most water molecules. Depending on the hydrogen bonding with neighbouring functional groups and with other water molecules, the OH bending mode can vary from 1589 cm^{-1} (non-hydrogen bonded) to 1650 cm^{-1} (strongly hydrogen bonded).[84] Vibrational frequencies between 1545 and 1589 cm^{-1} have also been attributed to OH bending modes of water molecules when electrons are stabilized at the hydrogen-terminated NDs-water interface.[47] More details related to water contribution in this region are given in section 5.1.

3.5. C=O stretching modes (1680-1860 cm^{-1})

Most pristine NDs have a broad absorption band at 1720-1780 cm^{-1} related to C=O stretching modes induced by oxidation treatments during the cleaning of the NDs from non-diamond carbon.[29,31,36,69,73,83,85–89] Depending on the chemical environment and the degree of oxidation, the C=O stretching vibrations can shift from 1680 to 1860 cm^{-1} (see Table 1 for details and references). Contributions from ketones, lactams, aldehydes and esters appear mainly around 1720-1740 cm^{-1} while carbonyl, cyclic ketones and carboxyl groups are shifted upwards to around 1740-1780 cm^{-1}. The C=O stretching frequencies shifts to higher wavenumbers with the formation of lactones (1787-1795 cm^{-1}), saturated (1800-1810 cm^{-1}) and cyclic anhydride (up to 1858 cm^{-1}) structures because of stronger oxidation. However the C=O stretching band also undergoes shifts to higher wavenumbers with increasing of the size of the NDs, which was attributed to hydrogen bonding between neighbouring carboxylic groups.[36] A direct comparison between C=O stretching frequencies from NDs produced by different synthesis processes should therefore be performed with care.

3.6. Phonon bands (1800-2600 cm^{-1})

Two-phonon absorption in bulk diamond appears as several absorption bands between 1800 and 2600 cm^{-1}.[90] Although the two-phonon signature was still recorded for diamond particles down to 500 nm in size,[66] it was not detected for NDs with smaller sizes, due to the phonon confinement effects.[31] Bands observed in FTIR spectra around 2300-2400 cm^{-1} are generally resulting from incomplete CO_2 purging of the spectrometers and are not related to NDs.

3.7. CH_x stretching bands (2830-2960 cm^{-1})

The crystallinity difference between 5 nm sized NDs (detonation or meteoritic) and larger NDs of 100 nm dramatically influences the CH stretching vibrations of NDs.[37] For the 100 nm NDs, sharp features associated with C-H bonds on mainly C(111), but also C(100) and C(110) facets have been identified (see table 1)[35,37] similarly as for the case of bulk diamond.[91,92] On the other hand, two broad bands are usually observed for smaller 5 nm sized NDs, which are associated with symmetric and asymmetric stretching modes of the various CH_x groups.[13,47,69,70,74] Note that NDs are highly sensitive to hydrocarbon contamination, which can complicate the interpretation of CH stretching bands without *in situ* preparation or annealing in vacuum.[37,74,93]

3.8. NH_x stretching bands (3050-3450 cm^{-1})

NH_x stretching mode frequencies are dependent on the type of amino groups and intermolecular hydrogen bonding with neighbouring groups.[76,77,80,94] They strongly overlap with OH stretching modes from water molecules but can be discriminated by annealing under vacuum as discussed in section 4.5.[76]

3.9. OH stretching bands (3200-3600 cm^{-1})

The OH stretching bands appear as a broad band between 3200-3600 cm^{-1} that can either be attributed to adsorbed water or hydroxyl groups on NDs. [10,12,14,74,76,83] More details on the different components are discussed in section 4.2 and 5.1.

***Table 1**: Overview of reported spectral assignments of NDs FTIR spectra.*

Absorbance frequency (cm^{-1})	Assignment	Type of NDs[a]	FTIR method[b]	References
709	C-Cl	DND	-	[71]
843	C-Cl	DP	DRIFT	[80]
940	C-O-C stretching, acid anhydride	HPHT ND	DRIFT (N_2)	[75]
959-969	CCC bending, COC symmetric stretching	DND	KBr	[31]
1043-1049	C-O bending, hydroxyl	DND, DND	KBr (air, vac.)	[31,74]
1050-1150	C-O stretching, hydroxyl and ether	HPHT ND	DRIFT (N_2)	[75]
1100-1140	C-O-C asymmetric bending, ether, ester, lactone, acid anhydride	DND	KBr, Si (air, vac.)	[31,69,72,73, 95]
1090-1140	C-O stretching, hydroxyl	DND	KBr (air, vac.), GAR	[10,63,73,74]
1180	N-induced on-phonon process	DND	KBr	[31]
1210, 1320	Amide III	DND	DRIFT, KBr (air, vac.)	[61,76,77]
1235-1245	C-N stretching	DND	DRIFTS	[61]
1254-1270	C-O bending, epoxy, ester	DND	KBr	[10,31,73,74, 96]
1260	Nitrogen A-defect	DND	KBr	[29,31]
1290	C-O stretching, carboxylic anhydride	HPHT ND	DRIFT (N_2)	[75]
1332	C-C stretching vibration of the diamond lattice	DND	KBr, ATR, DRIFT	[13,48,68–71]
1320-1370, 1410	C=O symmetric stretching, deprotonated carboxyl	DND, HPHT ND, DP	Si, ATR	[36,96]
1340	C-F stretching	DND	ATR	[97]
1360	N-induced on-phonon process	DND	KBr	[31]
1370	C-O stretching, carboxylic anhydride	HPHT ND	DRIFT (N_2)	[75]
1460-1470	CH_x asymmetric bending	DND	KBr, ATR (air, N_2)	[31,36,47,49, 50,69,70,74]

1514	N-H scissor	DP	DRIFT	[80]
1535	CN stretch (amide II)	DND		[79]
1535-1595	C=C stretching	DND, HPHT ND	KBr, DRIFT, ATR, GAR	[19,50,61,63, 74,82]
1545-1589	OH bending, water molecule close to an excess electron	DND	ATR	[47]
1555	C=O asymmetric stretching, deprotonated carboxyl	DND	Si	[36]
1610	C=N stretching	DP	DRIFT	[80]
1620-1640	OH bending, hydroxyl or water	DND, HPHT ND	KBr (air, vac.), ATR	[10,12,14,47, 49,74,76,83]
1630	OH bending water, C-O bending (amide II)	DND	KBr	[31,69]
1650, 1664	C=O stretching of amide I	DND	KBr	[69,77]
1680-1780	C=O stretching, deprotonated carboxyl, size dependent	DND, HPHT ND, DP	Si	[36]
1710-1725	C=O stretching, ketone, aldehydes	DND	KBr, ATR, Reflection	[47,50,69,85, 89,98]
1730-1820	C=O stretching, protonated carboxyl, size dependent	DND, HPHT ND, DP	Si	[31,36,72,88]
1728-1750	C=O stretching, carbonyl, ester	DND	KBr	[69,86]
1759	C=O stretching, lactam	DND	KBr	[31]
1783	C=O stretching, cyclic ketones	DND	KBr	[31,86]
1787, 1795	C=O stretching, lactone	DND	KBr, reflection	[88,89]
1790	C=O stretching, carboxylic anhydride	HPHT ND	DRIFT (N_2)	[75]
1795, 1813	C=O stretching, saturated anhydride	DND	KBr	[85,86]
1858	C=O stretching, cyclic acid anhydride	DND	Reflection (N_2)	[89]
1959	C-NH_3^+	DND	KBr (air, N_2)	[76]
2070-2180	C-D	DP	DRIFTS	[68]
2110	C-D stretching on C(111)-1x1	HPHT ND	Si (N_2)	[35]
2100-2200	C≡N stretching	DND	DRIFTS	[61]
2800-3500	N-H stretch	DND	KBr	[77]
2835	C(111)-1x1 plane C-H stretching	HPHT ND	Si (vac., N_2)	[35,37]
2845	C(110):H	HPHT ND	Si (vac.)	[37]
2850-2855	CH_2 symmetric stretching	DND	KBr	[31,69]
2857	C(110):H	HPHT ND	Si (vac.)	[37]
2870-2880	CH_3 symmetric stretching	DND	KBr	[31,69]
2885	C-H stretching	DND	KBr	[69]
2900	C_{sp3}-H	SC, DND	Si (vac.), ATR	[36,47,99]
2916	C(100):H	HPHT ND	Si (vac.)	[37]
2921	(100) C-H stretching	HPHT ND	Si (N_2)	[35]
2930	C(100):H	HPHT ND	Si (vac.)	[37]
2920-2930	CH_2 asymmetric stretching	DND	KBr	[31,69]
2940-2955	CH_3 asymmetric stretching	DND	KBr	[31,69]
3050,3088	Symmetric NH stretching	DND, DP	DRIFT, ATR	[80,94]
3152, 3280	Asymmetric NH stretching	DND, DP	DRIFT, ATR	[80,94]

3240	OH stretching, ice-like water with strong intermolecular bonding	DND	KBr	[31]
3240	N-H stretching	DND	KBr	[31]
3300-3500	OH stretching, hydroxyl	DND	KBr (air, vac.)	[10,12,14,74, 76,83]
3400	N-H symmetric stretching	DND	KBr (air, vac.)	[76]
3410-3425	OH stretching, liquid-like water or water on Lewis basic sites	DND	KBr	[31]
3490	N-H asymmetric stretching	DND	KBr (air, vac.)	[76]
3575-3590	OH stretching, gas-like water or water on Lewis acid sites	DND	KBr	[31]
3690-3695	OH stretching from isolated water	DND	ATR (air)	[47,49,71]

[a] Description of NDs type if available. DND: detonation NDs, HPHT NDs: High Pressure High Temperature NDs, DP: Diamond particle, diameter <500 nm [b] Si: Transmission after drying on Si substrate, KBr: Transmission through KBr pellet, ATR: Attenuated Total Reflectance, DRIFTS: Diffuse Reflectance, GAR: Grazing Angle Reflectance. If available, the atmospheric conditions of the experiment are also given (Vac.: vacuum, N_2: nitrogen).

4. FTIR spectra of surface-modified nanodiamonds

Homogenization of NDs surface chemistry is a critical step to ensure reproducible surface functionalization.[8] Due to its high sensitivity to surface functional groups, FTIR spectroscopy is a method of choice to validate the modifications of NDs surface chemistry after surface treatments. In this section, typical FTIR spectra of NDs after various surface treatments are summarized.

4.1. Oxidation

Chemical oxidation with a strong acid such as HNO_3/H_2SO_4 (1:1) mixture is the most commonly used method to etch amorphous and graphitic carbon around NDs from detonation soot.[83,87,88] It results in the formation of C=O bonds clearly identified by their stretching modes in the region 1720-1780 cm^{-1} (Figure 2a). The C=O stretching mainly refer to carboxylic acids and carbonyls but other groups are also contributing as discussed previously. In general, the C=O stretching band is shifted towards higher frequencies with increasing of the level of oxidation.

Annealing under air (at temperatures usually in the range of 200-600 °C) is an alternative treatment to oxidize the NDs surface and etch non-diamond carbon.[29,69,82,86,100] As a result, C=O stretching modes shift to higher frequencies by 20-40 cm^{-1} due to the conversion of ketones, aldehydes and ester groups into carboxylic and cyclic ketones. Carboxylic anhydride should appear at 1820 cm^{-1} which is outside the C=O range observed for the case of DNDs and was therefore ruled out.[69] On the other hand, on the surface of HPHT NDs, the air oxidation leads mainly to the formation of hydroxyl and ether groups with a strong C-O stretching band around 1100 cm^{-1}, with some carboxyl anhydride groups.[75] The disappearance of CH_x bands, if initially present on the surface, was also reported after air oxidation.[69,82,95]

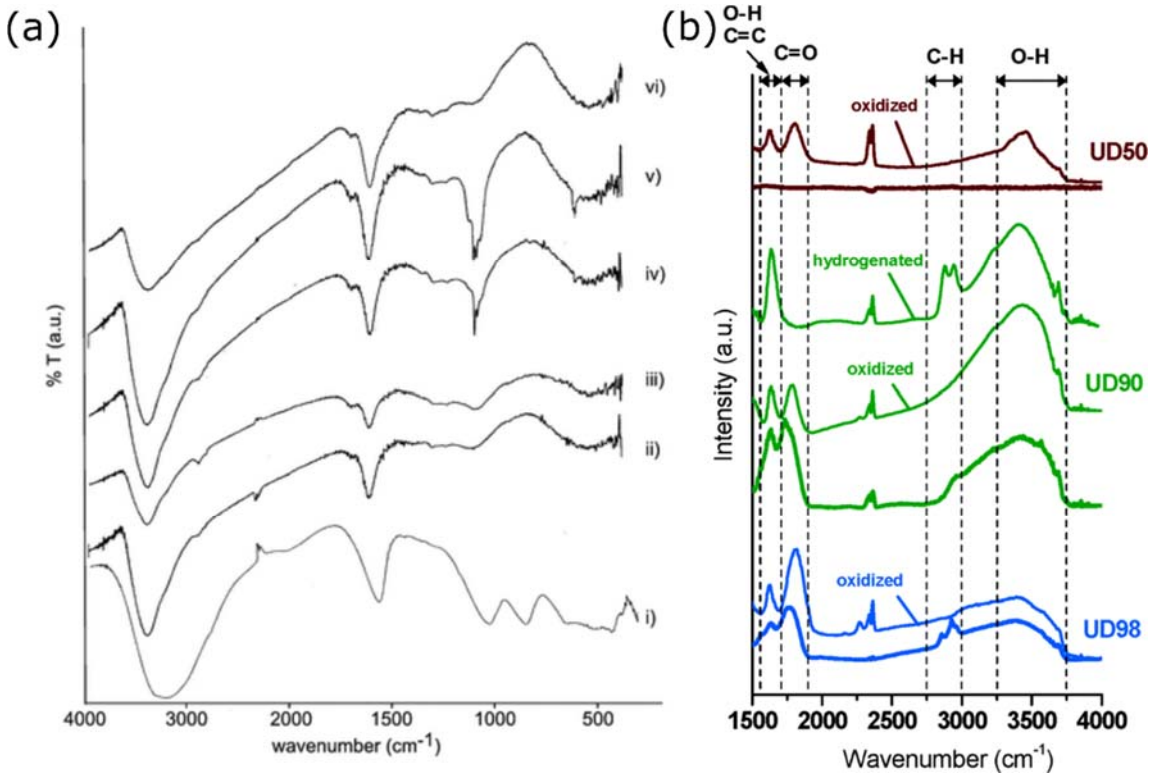

Figure 2: (a) FTIR spectra of NDs resulting from different chemical oxidation and reduction treatments: (i) after $LiAlH_4$ reduction, (ii) after reduction with borane, (iii) pristine, (iv) after oxidation with $HClO_4$, (v) after oxidation with HNO_3/H_2SO_4 and (vi) after reaction with ozone under UV irradiation. Reprinted with permission from reference [83]*. Copyright 2006 Royal Society of Chemistry. (b) FTIR spectra of NDs before (no label) and after (oxidized) thermal oxidation under air for 5 h at 425 °C for detonation soot (UD50, brown) and NDs purified by acid treatments (UD90, green and UD98, blue). For the UD90, the FTIR spectrum of the oxidized sample after annealing for 2h at 800 °C in hydrogen is also shown (hydrogenated). Reprinted with permission from* [82]*. Copyright 2006 American Chemical Society.*

Annealing in ozone atmosphere is another possibility for strong oxidation of the NDs while using lower annealing temperatures (150-200 °C).[89,101] In contrast to annealing under air, Shenderova *et al.* reported that no carbonyl band at 1720 cm^{-1} could be observed in ozone-treated NDs.[89] Instead, a strong band at 1858 cm^{-1}, attributed to cyclic acid anhydride groups, was detected in addition to lactone and hydroxyl contributions.

4.2. Hydroxylation

The formation of hydroxyl groups on the surface of NDs can be achieved by chemical reduction with borane or $LiAlH_4$,[74,76,83] Fenton reaction,[10,14] or irradiation with UV under ozone atmosphere.[12,83] Examples of FTIR spectra of hydroxylated NDs are shown in Figure 2a and 3. A strong increase in intensity of the OH bending and stretching vibrations is observed after hydroxylation. Note that the C=O stretching band disappears or is strongly reduced after borane or $LiAlH_4$ chemical reduction, whereas after Fenton reaction C=O bands are not affected.

OH vibrations coming from hydroxyl groups on the NDs surface or from water molecules are difficult to differentiate when the NDs-OH are characterized in ambient condition, especially since hydroxylated surfaces are highly hydrophilic. FTIR characterization under vacuum after mild annealing to remove water adsorbates enables the distinction between hydroxyl groups and water contributions

due to their different temperature stability (Figure 3b).[74] A broad band at 3300-3500 cm^{-1} remains after water desorption in vacuum for NDs-OH, which is not the case for oxidized NDs.

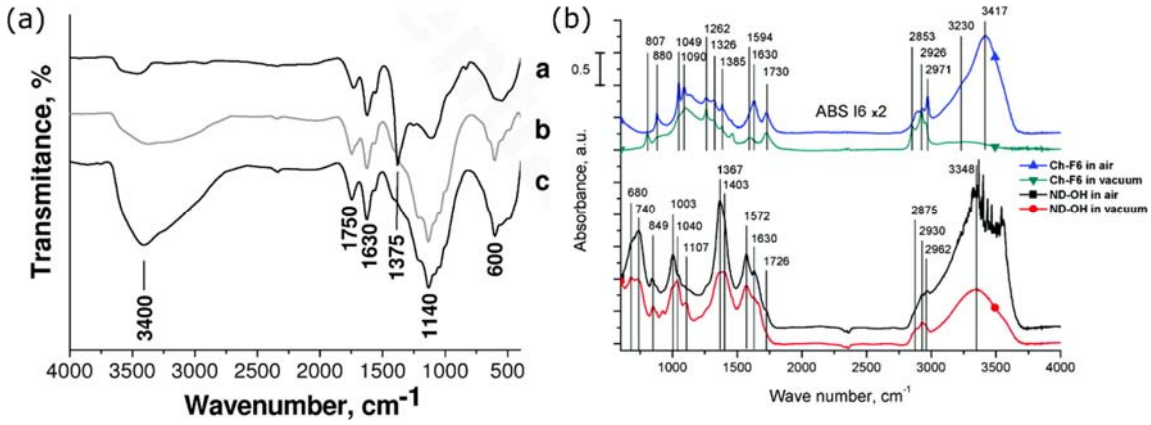

Figure 3: (a) FTIR spectra of pristine (top), moderate (middle) and deep (bottom) Fenton-treated DNDs. Reprinted with permission from reference [10]*. Copyright 2009 American Chemical Society. (b) FTIR spectra of pristine (Ch-F6) and hydroxylated (ND-OH) DNDs using $LiAlH_4$ reduction, characterized both in air and in vacuum after 200 °C annealing. Reprinted with permission from reference* [74]*. Copyright 2011 American Chemical Society.*

4.3. Hydrogenation

Hydrogenation of NDs can be achieved either by annealing under hydrogen atmosphere or by exposure to a hydrogen plasma.[13,31,35,37,70] This treatment leads to an intense increase of CH_x bending and stretching vibrations and reduction of C=O bands (Figure 4).[13,69–71] However, appearance of CH_x stretching bands should be treated with care since H-terminated NDs are strongly sensitive to hydrocarbon contamination, which can be difficult to separate from chemically bonded CH_x groups.[37,93] As already described earlier, on large NDs, sharp C-H signature over the different diamond facets should be detected,[35,37] while two broad bands are usually reported on DNDs.[13,70] A higher sensitivity to diamond C-C stretching band at 1332 cm^{-1} has also been observed for H-NDs,[13,49,70,71] which is associated with removal of oxygen-containing groups. Other bands appearing in the 1540-1670 cm^{-1} region have also been reported,[30,49,69,70] which have recently been attributed to OH vibrations of water molecules on H-NDs surface.[47]

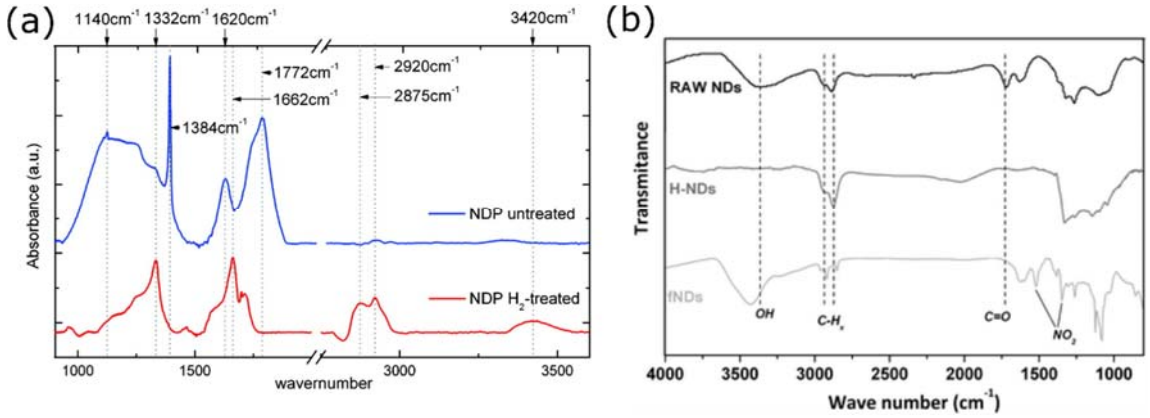

Figure 4: (a) FTIR spectra of as received DNDs (top) and after annealing under H_2 atmosphere. Reprinted with permission from [70]*. Copyright 2010 American Chemical Society. (b) FTIR spectra of as received DNDs (top), after H_2 plasma treatment (middle) and functionalization with diazonium (bottom). Reprinted with permission from reference* [13]*. Copyright 2011 Royal Society of Chemistry.*

4.4. Thermal reduction and graphitization

Annealing in inert atmosphere (argon, nitrogen) or in vacuum at moderate temperatures (<1000 °C) leads to desorption of surface functional group and eventually to the surface graphitization of the NDs surface.[9,69,100,102] The FTIR signature of NDs annealed in vacuum is quite similar to NDs annealed under molecular hydrogen, with a drastic reduction of C=O bands and an increase of CH_x stretching modes.[69] The H_2 atmosphere is however more reductive since lower temperatures are required to obtain similar FTIR spectra.[69] Strong C-O stretching bands around 1100 cm^{-1}, possibly coming from ether or epoxy groups, are still observed on the surface of NDs after annealing under vacuum above 700 °C and may come from binding of oxygen atoms from water and/or molecular oxygen on sp^2 reconstructions after exposure to air.[95] The appearance of C=C stretching bands is usually not reported despite surface graphitization, therefore Raman spectroscopy is more relevant than FTIR for characterization of sp^2-hybridized reconstructions on NDs.

4.5. Amination

The direct amination of NDs is reported to be a difficult reaction,[8] but several indirect amine grafting methods have been demonstrated.[15,76,77,80,94] The FTIR signature of NDs-NH_2 is mainly related to amine stretching and bending vibrations (Figure 5). Stretching vibrational modes were reported in the 3050-3450 cm^{-1} region, depending on the type of amino groups and intermolecular hydrogen bonding with neighbouring groups.[76,77,80,94] This region overlaps with OH stretching modes from water molecules but dehydrated FTIR spectra were reported by Hens *et al.* (Figure 5a).[76] N-H bending mode appears at 1630 cm^{-1}, similar to O-H bending mode. Further N-related groups related to amination treatment, such as N-H scissoring mode (1514 cm^{-1}), C=N (1610 cm^{-1}) or C-NH_3^+ (1959 cm^{-1}) were also reported.[76,80] Grafting ethylenediamine on carboxylated NDs surface results in the appearance of amide I (1665 cm^{-1}), II (1550 cm^{-1}) and III (1217-1317 cm^{-1}) in the spectra of NDs-NH_2 as reported by Mochalin *et al.* (Figure 5b).[77]

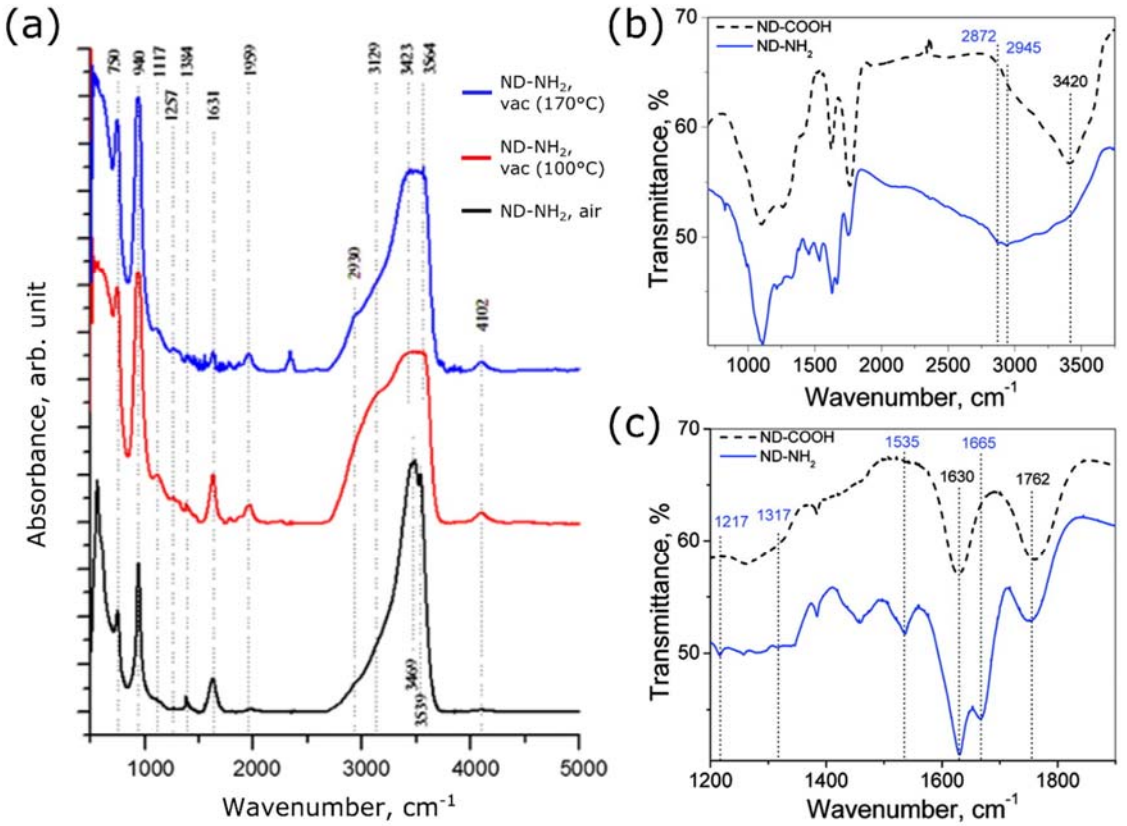

Figure 5: (a) FTIR spectra of aminated DNDs characterized in air (black) and under vacuum at 100 °C (red) and 170 °C (blue). Adapted with permission from reference [76]*. Copyright 2008 Elsevier. (b) Comparison between carboxylated (dashed) and aminated (full) NDs in the whole MIR region (a) and the region of amide bands (b). Adapted with permission from reference* [77]*. Copyright 2011 American Chemical Society.*

4.6. Other surface treatments

Fluorination of DNDs is usually validated by C-F stretching vibrations appearing in the region 1100-1400 cm^{-1} and bands at 1700-1870 cm^{-1} attributed to C=O stretching modes of F-substituted carbonyl groups.[48,94] In parallel, a strong decrease of OH vibrations was reported. Chlorination leads to the formation of a distinctive C-Cl bond which was reported at 709 or 843 cm^{-1} depending on the size of nanoparticles.[71,80]

5. *In situ/Operando* FTIR characterization of nanodiamonds

5.1. Influence of water on FTIR spectra of nanodiamonds

Simple exposure of NDs to ambient air can induce dramatic changes in the FTIR spectra due to water adsorption.[30,69] In addition to appearance of new peaks, the intensity and the vibrational frequencies of the bands coming from the surface groups can also change. When characterizing the surface chemistry of NDs, these effects can be minimised by performing FTIR measurements in vacuum. The high sensitivity of FTIR to water molecular vibrations, especially OH bending and

stretching modes, has however been utilised for more detailed studies of water interactions with NDs surface.[30,47,49] A seminal work by Ji *et al.* identified different types of water adsorption sites on the NDs, with adsorption profiles being strongly dependent on NDs surface functional groups.[30]

Since the OH stretching and bending modes are highly sensitive to hydrogen bonding between water molecules, it has been used for more detailed studies of hydrogen bonded network in different materials.[84,103–105] For NDs, both transmission through KBr pellets and ATR measurements were performed on NDs exposed to water molecules, generally in vapour phase. Due to their high hydrophilicity, multilayer water adsorption is usually observed upon exposure of NDs to ambient or humid air.[30,74]

The OH stretching bands of non-hydrogen-bonded water has been reported on H-terminated NDs as one or two sharp peaks at 3960-3965 cm^{-1} and 3620 cm^{-1}.[47,49,71,106] Vibrations around 3575 cm^{-1} were attributed to weak water adsorption at Lewis acid sites while stronger water adsorption at Lewis basic sites was proposed as the origin of the strongest band around 3412 cm^{-1}.[30] Additionally, intermolecular bonding between water molecules was attributed to the component at lower frequency (3240 cm^{-1}). However these last three bands can also be interpreted in terms of water with poorly connected, liquid-like and ice-like hydrogen bonded structures, respectively,[47] by analogy with studies performed on water hydrogen bonded network in other materials.[103–105]

The OH bending mode can also provide information about the strength of hydrogen bonding between the NDs surface and surrounding water molecules.[84] For most NDs, a single peak at 1620-1640 cm^{-1} is detected, related to hydrogen-bonded water molecules similar to liquid water. However, for the case of hydrogenated NDs the shift to lower frequencies (~1616 cm^{-1}) was observed which implies the OH bonds having weaker hydrogen bonding that can be related to water adsorption on hydrophobic sites (Figure 6).[47,49] When exposed to humid air *in situ*, some of the OH vibrations were reported shifted as far down as 1545 cm^{-1}, even below the vibrational mode of non-hydrogen bonded water molecule appearing at 1590 cm^{-1}. This contribution was attributed to OH vibration of water molecules close to an excess electrons trapped at the diamond-water interface.[47]

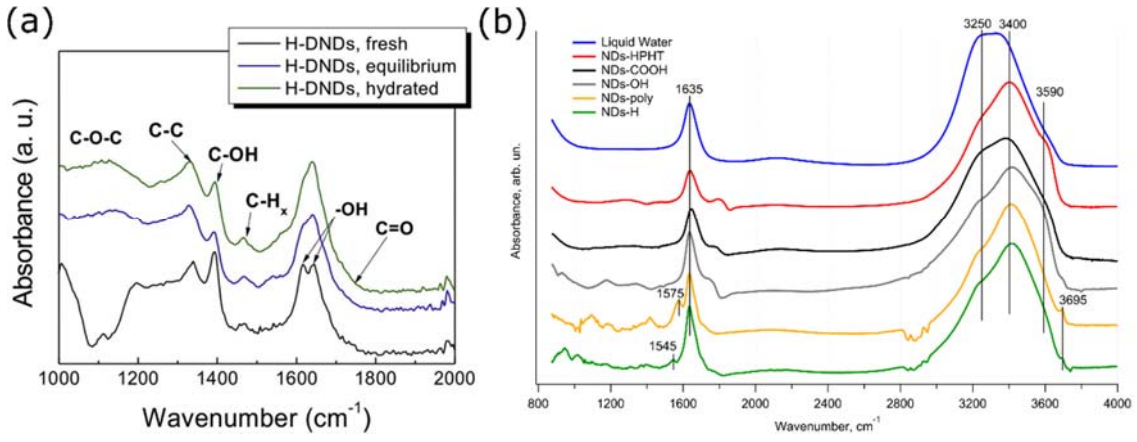

Figure 6: (a) ATR-FTIR spectra of H-DNDs in dry state (black), after equilibrium at ambient conditions (blue) and after dispersion in water (green). Reprinted with permission from reference [49]*. Copyright 2016 Elsevier. (b) Difference FTIR spectra between NDs with various surface chemistry in dry state and after exposure to humid air. Reprinted with permission from reference* [47]*. Copyright 2017 American Chemical Society.*

On oxidized NDs surfaces, the C=O stretching band is also affected by water adsorption.[36,47] Tu *et al.* proposed that large redshifts of the C=O stretching band could be expected after hydrogen bonding

with water molecules.[36] In addition, they reported redshifts of up to 50 cm^{-1} between basic and acidic pH due to the deprotonation of carboxyl groups. Redshifts of 6-7 cm^{-1} as well as a small decrease in absorbance were detected on carboxylated NDs after exposure to humid air.[47] The presence of adsorbed water as well as the initial pH of the dispersion, if dispersed before a measurement, should therefore be taken into account when interpreting the C=O stretching band frequency. Finally, small intensity changes of the CH_x stretching band absorbance were detected after exposure to water on H-NDs (Figure 6b), which origin remains unclear.[47]

Fewer studies have also been published on other solvent molecules. *In situ* exposure of NDs to ethanol using ATR FTIR was recently reported.[46] Inel *et al.* have shown that ethanol molecules adsorb preferentially with the –OH group oriented towards the NDs surface thus forming hydrogen bonds with C=O groups from carboxylic acids or acid anhydrides. Exposure of NDs to other types of solvent would certainly provide further insights into solvation properties of NDs.

5.2. Electrochemical processes at the surface of nanodiamonds

Electrochemical processes occurring at the surface of NDs in aqueous medium have been followed using ATR FTIR as shown by the work of Holt and co-workers.[50,107] For example, the electrochemical response of the ND spectral features in the presence of the redox species $IrCl_6^{2-}$ was investigated after drop casting detonation NDs on a diamond ATR crystal.[50] *In situ* FTIR measurements in 10 µM aqueous solution of $IrCl_6^{2-}$ followed the modifications occurring on the NDs surface chemistry over time (Figure 7a). Decrease in the absorbance intensity of C-OH stretching band of alcohol group at 1072 cm^{-1} and corresponding increase of a band at 1665 cm^{-1} associated to carbonyl quinone-like surface groups was interpreted in terms of electron transfer between $IrCl_6^{2-}$ and NDs surface, leading to oxidation of alcohols to carbonyls. Absorbance intensity losses at 1732 and 1288 cm^{-1} were also observed in solutions in the absence of $IrCl_6^{2-}$ ions demonstrating that they are not related to a redox process. In addition, both processes underwent an intensity decay with different temporal profiles demonstrating the importance of *in situ* measurements over time for tracking complex electrochemical processes at the surface of NDs in aqueous medium.

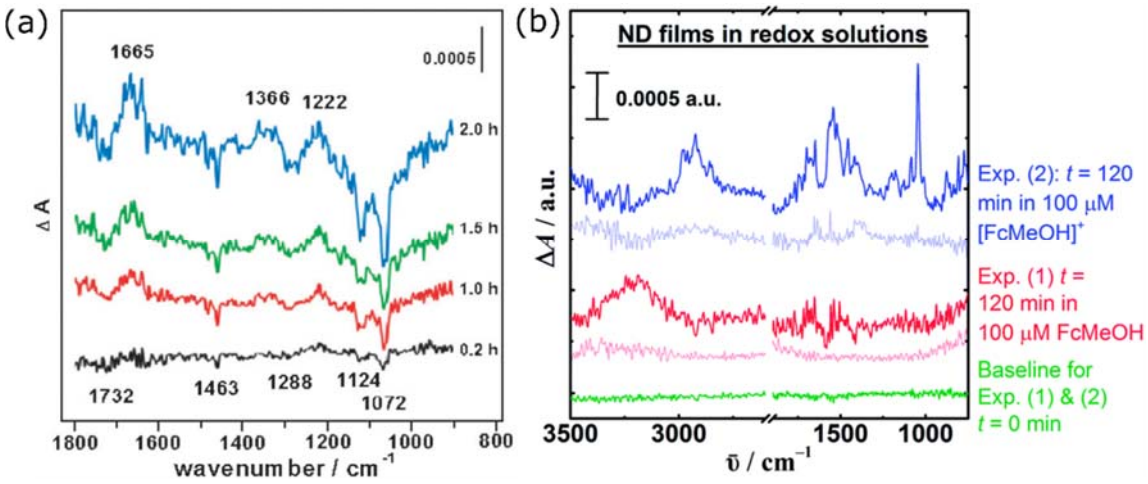

Figure 7: (a) ATR FTIR difference spectra of NDs exposed to 10 µM $IrCl_6^{2-}$ compared to equilibrated sample in 0.1M NaCl at pH 4 over time. Reprinted with permission from reference [50]*. Copyright 2011 Royal Society of Chemistry. (b) FcMeOH (red) and $FcMeOH^+$ (blue) on a clean ATR prism (transparent*

line), and in the presence of NDs (solid line). All aqueous solutions contained KCl (0.1 M, pH 5.88). Reprinted with permission from reference [107]*. Copyright 2014 Royal Society of Chemistry.*

Interactions between NDs and ferrocene methanol (FcMeOH) redox species in aqueous solution were also investigated.[107] After exposure to FcMeOH for 120 min slight increase of the absorbance intensity of OH stretching and bending modes are reported, while appearance of new bands, mostly associated with FcMeOH signature, are observed after exposure to $FcMeOH^+$ (Figure 7b). This difference is mainly illustrating electrostatic adsorption of positively charged ions compared to neutral ones on the surface of NDs, which could support cyclic voltammetry data in understanding of NDs-FcMeOH electrochemical interactions.

5.3. Catalytic processes at the surface of nanodiamonds

Catalytic (and photocatalytic) processes occurring at the surface of nanoparticles had been monitored using FTIR, mainly in the DRIFT mode.[57,58] Su and co-workers demonstrated that this technique is sensitive to changes of the NDs surface chemistry during catalytic processes.[60–62] In addition, FTIR can also be used to monitor the evolution of the reactants during the catalytic reaction. For example, the dehydrogenation of ethylbenzene on NDs was followed at temperatures up to 450 °C (Figure 8a).[62] C=O groups were identified as a key functional group for the catalytic process which is activated during the reaction, as evidenced by a shift from 1790 to 1765 cm^{-1} of the C=O stretching band measured *in operando* during the temperature increase. Appearance of OH stretching bands was attributed to the formation of hydroxyl-like intermediates. On the other hand, C-H stretching bands and skeletal C-C bonds of ethylbenzene did not undergo any change, suggesting that the benzene molecules have poor interactions with the NDs. [62] Carbonyl and surface defects leading to the appearance of OH groups were found to play a role in the adsorption of borate on NDs, influencing their catalytic reactivity towards the dehydrogenation of propane.[60] In this case, the DRIFT spectra were recorded *in situ* at 230 °C in helium to eliminate any contribution from water adsorbates.

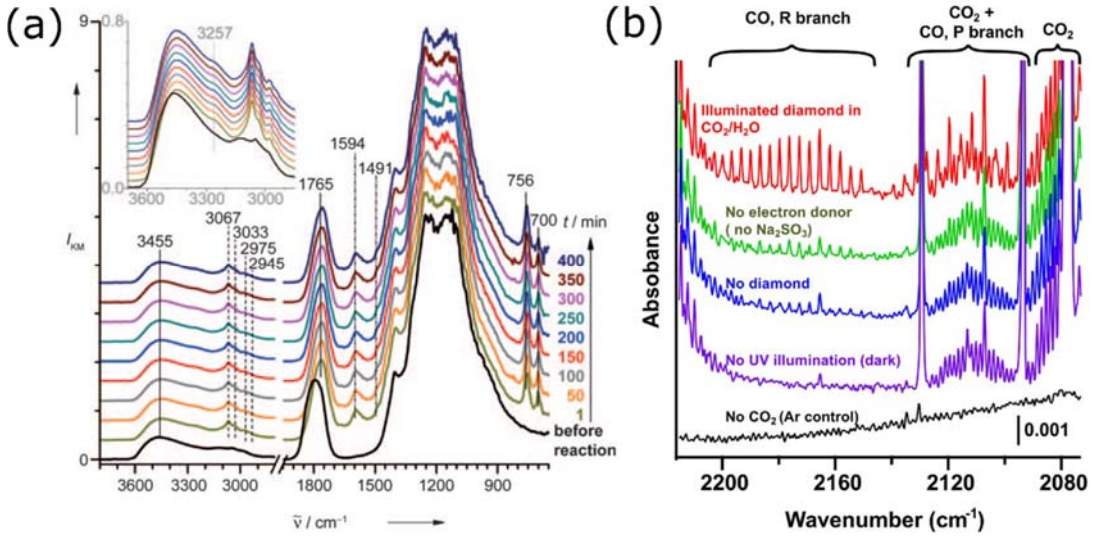

Figure 8: (a) DRIFT spectra of NDs catalysts under a flow of diluted ethylbenzene at 450°C. Reprinted with permission from reference [62]. *Copyright 2010 Wiley. (b) Transmission FTIR of gas-phase products after UV illumination of NDs in CO_2-saturated water with 125 µM SO_3^{2-}/SO_4^{2-} and respective control experiments. Reprinted with permission from reference* [108]*. Copyright 2017 Elsevier.*

FTIR can also be used to characterize gas-phase products generated by photocatalytic reactions on NDs, such as CO_2 reduction under UV illumination.[108] Even if these measurements are not directly probing the NDs surface, indirect information concerning chemical reactions occurring at the surface of NDs can be determined by recording FTIR spectra of formed end products (Figure 8b). In particular, control experiments demonstrated the need for CO_2, UV illumination and an electron donor such as Na_2SO_3 to achieve significant photoreduction of CO_2 to CO induced by NDs [108].

6. Future perspectives

Most FTIR characterizations of NDs so far have been performed using KBr pellets either held at ambient or under vacuum conditions using transmission mode. Although this method has been very successful, care has to be taken that the correct background correction is chosen and consistent sample preparation is needed for the quantitative investigation and comparison between the measurements of different groups and different methods. More studies performed in carefully controlled environments, such as UHV conditions, would certainly enrich the interpretation of FTIR spectra of NDs with defined surface groups. Comparison of FTIR spectra from NDs having different structural properties (size, purity…) but having been exposed to similar surface treatments would also be of high interest to better understand the chemical reactivity of NDs.

Current studies of NDs based on ATR and DRIFT are focusing on relatively large amounts of sample to increase the surface area, and hence the number of surface functional groups, being probed by the IR light. In general, little information is provided regarding the surface area of the NDs samples in DRIFT or the thickness of the NDs films deposited on the crystal in ATR measurements. However, this information becomes important when investigating the reactions at the solid/liquid or solid/gas interfaces and consistent sample area/thickness are important for quantitative comparison. Good adhesion to an ATR crystal and an even distribution over the crystal area exposed to IR light are particularly important when the ND layer is exposed to a liquid solution or when electrical potential is applied as part of the electrode system. More information concerning the NDs film thickness, adhesion, distribution and stability would be beneficial for the development of *in situ* measurements and should be reported in future studies.

In situ ATR-FTIR and DRIFT studies on NDs started to emerge as we described in section 5. Although very challenging, *operando* measurements which have been demonstrated on other types of nanoparticles,[6] are also expected to gain in importance in NDs research as they would add invaluable information on chemical processes which cannot easily be followed with other spectroscopic techniques. To obtain the structural and kinetic information in NDs under realistic conditions, particularly when thin sample layers or monolayers are required, the correct combination of sensitivity and selectivity as well as time resolution of data collection are necessary. The limitation of IR in general is that the spectra can be complex to interpret as multiple species are often present on the surface of NDs which by nature have weak absorption intensities and vibrational modes with lower absorbance cross sections can be lost. Although rapid and step scan modes of FTIR spectrometers have time resolution on the micro to nanosecond scales, the temporal resolution of dynamics study may be compromised by averaging of the data to be able to detect very weak signals from the active species. In order to probe monolayers of NDs and reactions of their surface groups at the interfaces more advanced surface sensitive techniques would have to be used. Infrared reflection-absorption spectroscopy (IRRAS) is often applied to study monolayer thin films adsorbed on reflective metal substrates.[109] It is performed under grazing incidence and due to the surface selection rules it has high sensitivity ($<10^{-4}$ monolayers) to the vibrational modes with a component of their dipole change perpendicular to the metal surface. Additional modulation of the radiation polarization can increase

surface sensitivity and remove the strong influence of gas or bulk water adsorbed on NDs surfaces as achieved by the Polarization Modulation Infrared Reflectance Absorption Spectroscopy (PM-IRRAS).[110,111] Surface enhanced infrared spectroscopy (SEIRA) is another advanced method suitable for *in situ* and in operando studies of nanoparticles, for which 10–1000 times more intense adsorption intensities have been reported on metal surfaces[4,22], or even on some other materials such as graphene,[4] or double-layered nanoparticle stacks.[112]

The application of FTIR imaging could also become of interest for the NDs community, especially inside fixed cells or live cells for biomedical applications. ATR imaging[39,113] and FTIR microscopy using synchrotron sources[114–116] have lateral spatial resolutions in the range of several micrometers, which corresponds to the diffraction limit in the IR region. IR based techniques achieving nanometer scale spatial resolution have also been developing in recent years and are moving towards the single molecule sensitivity.[117,118] Based on either scattering-type scanning near field optical microscopy (s-SNOM) or photo thermal-effect (AFM-IR)[119,120] these imaging methods collect the IR spectra from the sample areas as low as 20 nm [117,121], either using the tunable laser sources or the broadband synchrotron sources.[122,123] In recent work using AFM-IR technique, the conformational changes in proteins inside biological cells were investigated following the uptake of NDs[124] and the sensitivity moving towards a single protein detection was reported by nano-FTIR.[125]

Spectral processing of the FTIR data such as deconvolution and derivative of the spectra can facilitate the estimation of the band positions and their relative contributions.[30,31,35,47,69] Statistical methods such as principal component analysis are often used to distinguish between subtle differences in large numbers of spectra, but also various correction methods to account for different distortion artefacts.[126,127] Two-dimensional (2D) correlation spectroscopy can provide additional information of the correlation and sequence of events recorded *in situ* or *in operando* methods as well as improved spectral resolution.[128,129] Theoretical methods have also been employed to aid the assignments of infrared peaks.[74,130] Although still poorly used by the NDs community, advanced data analysis methods and theoretical support may facilitate the interpretation of weak signal detected during *in operando* measurements.

7. Conclusions

FTIR is a powerful technique for the characterisation of the surface chemistry of NDs. The FTIR methods currently applied to NDs in various environment have been reviewed. The interpretation of FTIR spectra of NDs with defined surface chemistries is relatively well documented and a summary of the current assignments of features from FTIR spectra of NDs was provided. Nevertheless, there is still a need for more studies investigating systematically NDs with different preparation methods, size distribution and/or different sample environment. Early work on *in situ/operando* FTIR characterization of chemical processes at the interface between NDs and liquid and gases were presented. Although FTIR has already been used since several decades, the analytical methods are constantly evolving to be applied in more complex environment and offer higher time- and spatial-resolutions. FTIR would therefore remain an essential tool for the characterization of NDs surface chemistry both as complementary information to other methods such as Raman spectroscopy [131] and X-ray photoelectron spectroscopy [132] for example, and for the dynamic information when monitoring the reactivity of NDs in complex media in the future.

Acknowledgments

The authors acknowledge Ulrich Schade for fruitful discussions. T.P. acknowledges the Volkswagen Foundation (Freigeist Fellowship No. 89592) for financial support.

References

[1] V.N. Mochalin, O. Shenderova, D. Ho, Y. Gogotsi, The properties and applications of nanodiamonds, Nat. Nanotechnol. 7 (2012) 11–23. doi:10.1038/nnano.2011.209.

[2] O.A. Shenderova, G.E. McGuire, Science and engineering of nanodiamond particle surfaces for biological applications (Review), Biointerphases. 10 (2015) 030802. doi:10.1116/1.4927679.

[3] J.-C. Arnault, Nanodiamonds advanced material analysis, properties and applications, Elsevier, 2017.

[4] Á.I. López-Lorente, B. Mizaikoff, Recent advances on the characterization of nanoparticles using infrared spectroscopy, TrAC - Trends Anal. Chem. 84 (2016) 97–106. doi:10.1016/j.trac.2016.01.012.

[5] I.A. Mudunkotuwa, A. Al Minshid, V.H. Grassian, ATR-FTIR spectroscopy as a tool to probe surface adsorption on nanoparticles at the liquid-solid interface in environmentally and biologically relevant media., Analyst. 139 (2014) 870–81. doi:10.1039/c3an01684f.

[6] F. Zaera, New advances in the use of infrared absorption spectroscopy for the characterization of heterogeneous catalytic reactions, Chem. Soc. Rev. 43 (2014) 7624–7663. doi:10.1039/C3CS60374A.

[7] O. Shenderova, V. Zhirnov, D. Brenner, Carbon Nanostructures, Crit. Rev. Solid State Mater. Sci. 27 (2002) 227–356. doi:10.1080/10408430208500497.

[8] A. Krueger, D. Lang, Functionality is Key: Recent Progress in the Surface Modification of Nanodiamond, Adv. Funct. Mater. 22 (2012) 890–906. doi:10.1002/adfm.201102670.

[9] T. Meinhardt, D. Lang, H. Dill, A. Krueger, Pushing the Functionality of Diamond Nanoparticles to New Horizons: Orthogonally Functionalized Nanodiamond Using Click Chemistry, Adv. Funct. Mater. 21 (2011) 494–500. doi:10.1002/adfm.201001219.

[10] R. Martín, P.C. Heydorn, M. Alvaro, H. Garcia, General Strategy for High-Density Covalent Functionalization of Diamond Nanoparticles Using Fenton Chemistry, Chem. Mater. 21 (2009) 4505–4514. doi:10.1021/cm9012602.

[11] P.-H. Chung, E. Perevedentseva, J.-S. Tu, C.C. Chang, C.-L. Cheng, Spectroscopic study of bio-functionalized nanodiamonds, Diam. Relat. Mater. 15 (2006) 622–625. doi:10.1016/j.diamond.2005.11.019.

[12] H.A. Girard, T. Petit, S. Perruchas, T. Gacoin, C. Gesset, J.-C.C. Arnault, P. Bergonzo, Surface properties of hydrogenated nanodiamonds: a chemical investigation., Phys. Chem. Chem. Phys. 13 (2011) 11517–11523. doi:10.1039/c1cp20424f.

[13] J.-C. Arnault, T. Petit, H. Girard, A. Chavanne, C. Gesset, M. Sennour, M. Chaigneau, Surface chemical modifications and surface reactivity of nanodiamonds hydrogenated by CVD plasma., Phys. Chem. Chem. Phys. 13 (2011) 11481–11487. doi:10.1039/c1cp20109c.

[14] R. Martín, M. Álvaro, J.R.J.R. Herance, H. García, R. Martín, M. Alvaro, H. García, Fenton-Treated Functionalized Diamond Nanoparticles as Gene Delivery System, ACS Nano. 4 (2010) 65–74. doi:10.1021/nn901616c.

[15] A. Krueger, J. Stegk, Y. Liang, L. Lu, G. Jarre, Biotinylated Nanodiamond: Simple and Efficient

Functionalization of Detonation Diamond, Langmuir. 24 (2008) 4200–4204. doi:10.1021/la703482v.

[16] D. Lang, A. Krueger, The Prato reaction on nanodiamond: Surface functionalization by formation of pyrrolidine rings, Diam. Relat. Mater. 20 (2011) 101–104. doi:10.1016/j.diamond.2010.09.001.

[17] A. Barras, S. Szunerits, L. Marcon, N. Monfilliette-Dupont, R. Boukherroub, Functionalization of Diamond Nanoparticles Using “Click” Chemistry, Langmuir. (2010) 100726110923035. doi:10.1021/la101709q.

[18] L. Zhao, Y.H. Xu, T. Akasaka, S. Abe, N. Komatsu, F. Watari, X. Chen, Polyglycerol-coated nanodiamond as a macrophage-evading platform for selective drug delivery in cancer cells, Biomaterials. 35 (2014) 5393–5406. doi:10.1016/j.biomaterials.2014.03.041.

[19] Y. Liang, M. Ozawa, A. Krueger, A General Procedure to Functionalize Agglomerating Nanoparticles Demonstrated on Nanodiamond, ACS Nano. 3 (2009) 2288–2296. doi:10.1021/nn900339s.

[20] C.-C. Li, C.-L. Huang, Preparation of clear colloidal solutions of detonation nanodiamond in organic solvents, Colloids Surfaces A Physicochem. Eng. Asp. 353 (2010) 52–56. doi:10.1016/j.colsurfa.2009.10.019.

[21] W.-W. Zheng, Y.-H. Hsieh, Y.-C. Chiu, S.-J. Cai, C.-L. Cheng, C. Chen, Organic functionalization of ultradispersed nanodiamond: synthesis and applications, J. Mater. Chem. 19 (2009) 8432. doi:10.1039/b904302k.

[22] Chalmers John M. and Griffiths Peter R., Handbook of Vibrational Spectroscopy, John Wiley & Sons, Ltd, Chichester, UK, 2001. doi:10.1002/0470027320.

[23] J.S. Gaffney, N.A. Marley, D.E. Jones, Fourier Transform Infrared (FTIR) Spectroscopy, Charact. Mater. (2012) 1104–1135. doi:10.1002/0471266965.

[24] P.R. Griffiths, J.A. de Haseth, Fourier Transform Infrared Spectrometry, Second Edi, John Wiley & Sons, Inc., Hoboken, NJ, USA, 2007. doi:10.1002/047010631X.

[25] B.H. Stuart, Infrared Spectroscopy: Fundamentals and Applications, 2004. doi:10.1002/0470011149.

[26] E. Ritter, L. Puskar, F.J. Bartl, E.F. Aziz, P. Hegemann, U. Schade, Time-resolved infrared spectroscopic techniques as applied to channelrhodopsin., Front. Mol. Biosci. 2 (2015) 38. doi:10.3389/fmolb.2015.00038.

[27] W. Herres, J. Gronholz, Understanding FT-IR Data Processing, Part. 1 (1984) 352–356.

[28] H.G.M. Hill, L.B. D’Hendecourt, C. Perron, A.P. Jones, Infrared spectroscopy of interstellar nanodiamonds from the Orgueil meteorite, Meteorit. Planet. Sci. 32 (1997) 713–718. doi:10.1111/j.1945-5100.1997.tb01556.x.

[29] E. Mironov, A. Koretz, E. Petrov, Detonation synthesis ultradispersed diamond structural properties investigation by infrared absorption, Diam. Relat. Mater. 11 (2002) 872–876. doi:10.1016/S0925-9635(01)00723-3.

[30] S. Ji, T. Jiang, K. Xu, S. Li, FTIR study of the adsorption of water on ultradispersed diamond powder surface, Appl. Surf. Sci. 133 (1998) 231–238. doi:10.1016/S0169-4332(98)00209-8.

[31] T. Jiang, K. Xu, FTIR study of ultradispersed diamond powder synthesized by explosive detonation, Carbon N. Y. 33 (1995) 1663–1671. doi:10.1016/0008-6223(95)00115-1.

[32] G. Laufer, J.T. Huneke, B.S.H. Royce, Y.C. Teng, Elimination of dispersion-induced distortion in infrared absorption spectra by use of photoacoustic spectroscopy, Appl. Phys. Lett. 37 (1980) 517–519. doi:10.1063/1.91996.

[33] R. Prost, The influence of the christiansen effect on I.R. spectra of powders, Clays Clay Miner.

21 (1973) 363–368. doi:10.1346/CCMN.1973.0210512.

[34] W. Jacob, A. Von Keudell, T. Schwarz-Selinger, Infrared analysis of thin films: amorphous, hydrogenated carbon on silicon, Brazilian J. Phys. 30 (2000) 508–516. doi:10.1590/S0103-97332000000300006.

[35] H.-C. Chang, J.-C. Lin, J.-Y. Wu, K.-H. Chen, Infrared spectroscopy and vibrational relaxation of CHx and CDx stretches on synthetic diamond nanocrystal surfaces, J. Phys. Chem. 99 (1995) 11081–11088. doi:10.1021/j100028a007.

[36] J.-S.S. Tu, E. Perevedentseva, P.-H.H. Chung, C.-L.L. Cheng, Size-dependent surface CO stretching frequency investigations on nanodiamond particles., J. Chem. Phys. 125 (2006) 174713. doi:10.1063/1.2370880.

[37] C.L. Cheng, C.F. Chen, W.C. Shaio, D.S. Tsai, K.H. Chen, The CH stretching features on diamonds of different origins, Diam. Relat. Mater. 14 (2005) 1455–1462. doi:10.1016/j.diamond.2005.03.003.

[38] N.J. Harrick, TOTAL INTERNAL REFLECTION AND ITS APPLICATION TO SURFACE STUDIES, Ann. N. Y. Acad. Sci. 101 (2006) 928–959. doi:10.1111/j.1749-6632.1963.tb54948.x.

[39] S.G. Kazarian, K.L.A. Chan, ATR-FTIR spectroscopic imaging: recent advances and applications to biological systems, Analyst. 138 (2013) 1940. doi:10.1039/c3an36865c.

[40] Perkin Elmer, ATR accessories - An overview, Tech. Note. (2004) 1–4.

[41] Z. Remes, H. Kozak, B. Rezek, E. Ukraintsev, O. Babchenko, A. Kromka, H.A. Girard, J.-C. Arnault, P. Bergonzo, Diamond-coated ATR prism for infrared absorption spectroscopy of surface-modified diamond nanoparticles, Appl. Surf. Sci. 270 (2013) 411–417. doi:10.1016/J.APSUSC.2013.01.039.

[42] T. Frosch, K.L.A. Chan, H.C. Wong, J.T. Cabral, S.G. Kazarian, Nondestructive three-dimensional analysis of layered polymer structures with chemical imaging, Langmuir. 26 (2010) 19027–19032. doi:10.1021/la103683h.

[43] M. Bradley, F. Izzia, ATR in the Far-Infrared Region, Thermo Electron Corp. (2004).

[44] L.A. Averett, P.R. Griffiths, K. Nishikida, Effective path length in attenuated total reflection spectroscopy, Anal. Chem. 80 (2008) 3045–3049. doi:10.1021/ac7025892.

[45] S. Nunn, D. Ph, K. Nishikida, Advanced ATR Correction Algorithm, Thermo Fish. Sci. (2008) 1–4. doi:See https://www.thermo.com/eThermo/CMA/PDFs/Product/productPDF_57540.PDF.

[46] G.A. Inel, E.-M. Ungureau, T.S. Varley, M. Hirani, K.B. Holt, Solvent–surface interactions between nanodiamond and ethanol studied with in situ infrared spectroscopy, Diam. Relat. Mater. 61 (2016) 7–13. doi:10.1016/j.diamond.2015.11.001.

[47] T. Petit, L. Puskar, T.A. Dolenko, S. Choudhury, E. Ritter, S. Burikov, K. Laptinskiy, Q. Brzustowski, U. Schade, H. Yuzawa, M. Nagasaka, N. Kosugi, M. Kurzyp, A. Venerosy, H.A. Girard, J.-C. Arnault, E. Osawa, N. Nunn, O. Shenderova, E.F. Aziz, Unusual Water Hydrogen Bond Network around Hydrogenated Nanodiamonds, J. Phys. Chem. C. 121 (2017) 5185−5194. doi:10.1021/acs.jpcc.7b00721.

[48] E.M. Zagrebina, A. V. Generalov, A.Y. Klyushin, K. a. Simonov, N. a. Vinogradov, M. Dubois, L. Frezet, N. Mårtensson, A.B. Preobrajenski, A.S. Vinogradov, Comparative NEXAFS, NMR, and FTIR study of various-sized nanodiamonds: As-prepared and fluorinated, J. Phys. Chem. C. 119 (2015) 835–844. doi:10.1021/jp510618s.

[49] S. Stehlik, T. Glatzel, V. Pichot, R. Pawlak, E. Meyer, D. Spitzer, B. Rezek, Water interaction with hydrogenated and oxidized detonation nanodiamonds - Microscopic and spectroscopic analyses, Diam. Relat. Mater. 63 (2016) 97–102. doi:10.1016/j.diamond.2015.08.016.

[50] J. Scholz, A.J. McQuillan, K.B. Holt, Redox transformations at nanodiamond surfaces revealed

by in situ infrared spectroscopy., Chem. Commun. (Camb). 47 (2011) 12140–2. doi:10.1039/c1cc14961j.

[51] M. Aramesh, O. Shimoni, K. Ostrikov, S. Prawer, J. Cervenka, Surface charge effects in protein adsorption on nanodiamonds, Nanoscale. 7 (2015) 5726–5736. doi:10.1039/C5NR00250H.

[52] R. Nakamura, A. Imanishi, K. Murakoshi, Y. Nakato, In Situ FTIR Studies of Primary Intermediates of Photocatalytic Reactions on Nanocrystalline TiO 2 Films in Contact with Aqueous Solutions, J. Am. Chem. Soc. 125 (2003) 7443–7450. doi:10.1021/ja029503q.

[53] P. Kubelka, F. Munk, Ein Beitrag Zur Optik Der Farbanstriche, Zeitschrift Für Tech. Phys. 12 (1931) 593–601.

[54] P. Kubelka, New contributions to the optics of intensely light-scattering materials, J. Opt. Soc. Am. 38 (1948) 448–457.

[55] H. Li, M. Rivallan, F. Thibault-Starzyk, A. Travert, F.C. Meunier, Effective bulk and surface temperatures of the catalyst bed of FT-IR cells used for in situ and operando studies, Phys. Chem. Chem. Phys. 15 (2013) 7321. doi:10.1039/c3cp50442e.

[56] R.M. Rioux, J.D. Hoefelmeyer, M. Grass, H. Song, K. Niesz, P. Yang, G.A. Somorjai, Adsorption and co-adsorption of ethylene and carbon monoxide on silica-supported monodisperse Pt nanoparticles: Volumetric adsorption and infrared spectroscopy studies, Langmuir. 24 (2008) 198–207. doi:10.1021/la702685a.

[57] M.A. Newton, M. Di Michiel, A. Kubacka, M. Fernández-García, Combining time-resolved hard X-ray diffraction and diffuse reflectance infrared spectroscopy to illuminate CO dissociation and transient carbon storage by supported Pd nanoparticles during CO/NO cycling, J. Am. Chem. Soc. 132 (2010) 4540–4541. doi:10.1021/ja9107512.

[58] H. Sheng, H. Zhang, W. Song, H. Ji, W. Ma, C. Chen, J. Zhao, Activation of Water in Titanium Dioxide Photocatalysis by Formation of Surface Hydrogen Bonds: An In Situ IR Spectroscopy Study, Angew. Chemie Int. Ed. 54 (2015) 5905–5909. doi:10.1002/anie.201412035.

[59] D.J. Cumming, C. Tumilson, S.F. Taylor, S. Chansai, a V Call, J. Jacquemin, C. Hardacre, R.H. Elder, Development of a diffuse reflectance infrared Fourier transform spectroscopy (DRIFTS) cell for the in situ analysis of co-electrolysis in a solid oxide cell, Faraday Discuss. 182 (2015) 97–111. doi:10.1039/c5fd00030k.

[60] X. Sun, Y. Ding, B. Zhang, R. Huang, D.S. Su, New insights into the oxidative dehydrogenation of propane on borate-modified nanodiamond, Chem. Commun. 51 (2015) 9145–9148. doi:10.1039/C5CC00588D.

[61] Y. Lin, D. Su, Fabrication of Nitrogen-Modified Annealed Nanodiamond with Improved Catalytic Activity, ACS Nano. 8 (2014) 7823–7833. doi:10.1021/nn501286v.

[62] J. Zhang, D.S. Su, R. Blume, R. Schlögl, R. Wang, X. Yang, A. Gajović, Surface Chemistry and Catalytic Reactivity of a Nanodiamond in the Steam-Free Dehydrogenation of Ethylbenzene, Angew. Chemie Int. Ed. 49 (2010) 8640–8644. doi:10.1002/anie.201002869.

[63] S. Stehlik, M. Varga, M. Ledinsky, V. Jirasek, A. Artemenko, H. Kozak, L. Ondic, V. Skakalova, G. Argentero, T. Pennycook, J.C. Meyer, A. Fejfar, A. Kromka, B. Rezek, Size and Purity Control of HPHT Nanodiamonds down to 1 nm, J. Phys. Chem. C. 119 (2015) 27708–27720. doi:10.1021/acs.jpcc.5b05259.

[64] H. Kozak, O. Babchenko, A. Artemenko, E. Ukraintsev, Z. Remes, B. Rezek, A. Kromka, Nanostructured Diamond Layers Enhance the Infrared Spectroscopy of Biomolecules, Langmuir. 30 (2014) 2054–2060. doi:10.1021/la404814c.

[65] M.G. Rockley, Reasons for the distortion of the fourier-transformed infrared photoacoustic spectroscopy of ammonium sulfate powder, Chem. Phys. Lett. 75 (1980) 370–372. doi:10.1016/0009-2614(80)80533-1.

[66] T. Ando, S. Inoue, M. Ishii, M. Kamo, Y. Sato, O. Yamada, T. Nakano, Fourier-transform infrared photoacoustic studies of hydrogenated diamond surfaces, J. Chem. Soc. Faraday Trans. 89 (1993) 749. doi:10.1039/ft9938900749.

[67] M.G. Rockley, Volume 75, Chem. Phys. Lett. 75 (1980) 370–372.

[68] T. Ando, M. Ishii, M. Kamo, Y. Sato, Thermal hydrogenation of diamond surfaces studied by diffuse reflectance Fourier-transform infrared, temperature-programmed desorption and laser Raman spectroscopy, J. Chem. Soc. Faraday Trans. 89 (1993) 1783. doi:10.1039/ft9938901783.

[69] T. Jiang, K. Xu, S. Ji, FTIR studies on the spectral changes of the surface functional groups of ultradispersed diamond powder synthesized by explosive detonation after treatment in hydrogen, nitrogen, methane and air at different temperatures, J. Chem. Soc. Faraday Trans. 92 (1996) 3401. doi:10.1039/ft9969203401.

[70] O.A. Williams, J. Hees, C. Dieker, W. Jäger, L. Kirste, C.E. Nebel, Size-Dependent Reactivity of Diamond Nanoparticles, ACS Nano. 4 (2010) 4824–4830. doi:10.1021/nn100748k.

[71] B. V Spitsyn, J.L. Davidson, M.N. Gradoboev, T.B. Galushko, N. V Serebryakova, T.A. Karpukhina, I.I. Kulakova, N.N. Melnik, Inroad to modification of detonation nanodiamond, Diam. Relat. Mater. 15 (2006) 296–299. doi:10.1016/J.DIAMOND.2005.07.033.

[72] N. Gibson, O. Shenderova, T.J.M.J.M. Luo, S. Moseenkov, V. Bondar, a. Puzyr, K. Purtov, Z. Fitzgerald, D.W.W. Brenner, Colloidal stability of modified nanodiamond particles, Diam. Relat. Mater. 18 (2009) 620–626. doi:10.1016/j.diamond.2008.10.049.

[73] D. Mitev, R. Dimitrova, M. Spassova, C. Minchev, S. Stavrev, Surface peculiarities of detonation nanodiamonds in dependence of fabrication and purification methods, Diam. Relat. Mater. 16 (2007) 776–780. doi:10.1016/j.diamond.2007.01.005.

[74] O. Shenderova, A.M. Panich, S. Moseenkov, S.C. Hens, V. Kuznetsov, H.M. Vieth, Hydroxylated Detonation Nanodiamond: FTIR, XPS, and NMR Studies, J. Phys. Chem. C. 115 (2011) 19005–19011. doi:10.1021/jp205389m.

[75] A. Wolcott, T. Schiros, M.E. Trusheim, E.H. Chen, D. Nordlund, R.E. Diaz, O. Gaathon, D. Englund, J.S. Owen, Surface Structure of Aerobically Oxidized Diamond Nanocrystals., J. Phys. Chem. C. Nanomater. Interfaces. 118 (2014) 26695–26702. doi:10.1021/jp506992c.

[76] S.C. Hens, G. Cunningham, T. Tyler, S. Moseenkov, V. Kuznetsov, O. Shenderova, Nanodiamond bioconjugate probes and their collection by electrophoresis, Diam. Relat. Mater. 17 (2008) 1858–1866. doi:10.1016/j.diamond.2008.03.020.

[77] V.N. Mochalin, I. Neitzel, B. Etzold, A.M. Peterson, G. Palmese, Y. Gogotsi, Covalent Incorporation of Aminated Nanodiamond into an Epoxy Polymer Network., ACS Nano. (2011) null. doi:10.1021/nn2024539.

[78] A. Krüger, F. Kataoka, M. Ozawa, T. Fujino, Y. Suzuki, A.E.E. Aleksenskii, A.Y. Vul', E. Ōsawa, Unusually tight aggregation in detonation nanodiamond: Identification and disintegration, Carbon N. Y. 43 (2005) 1722–1730. doi:10.1016/j.carbon.2005.02.020.

[79] Q. Zhang, V.N. Mochalin, I. Neitzel, I.Y. Knoke, J. Han, C. a Klug, J.G. Zhou, P.I. Lelkes, Y. Gogotsi, Fluorescent PLLA-nanodiamond composites for bone tissue engineering., Biomaterials. 32 (2011) 87–94. doi:10.1016/j.biomaterials.2010.08.090.

[80] K.-I. Sotowa, T. Amamoto, A. Sobana, K. Kusakabe, T. Imato, Effect of treatment temperature on the amination of chlorinated diamond, Diam. Relat. Mater. 13 (2004) 145–150. doi:10.1016/J.DIAMOND.2003.10.029.

[81] O. Shenderova, V. Grichko, S. Hens, J. Walch, Detonation nanodiamonds as UV radiation filter, Diam. Relat. Mater. 16 (2007) 2003–2008. doi:10.1016/j.diamond.2007.05.010.

[82] S. Osswald, G. Yushin, V. Mochalin, S.O. Kucheyev, Y. Gogotsi, Control of sp2/sp3 Carbon Ratio

and Surface Chemistry of Nanodiamond Powders by Selective Oxidation in Air, J. Am. Chem. Soc. 128 (2006) 11635–11642. doi:10.1021/ja063303n.

[83] A. Krueger, Y. Liang, G. Jarre, J. Stegk, Surface functionalisation of detonation diamond suitable for biological applications, J. Mater. Chem. 16 (2006) 2322. doi:10.1039/b601325b.

[84] M. Laporta, M. Pegoraro, L. Zanderighi, Perfluorosulfonated membrane (Nafion): FT-IR study of the state of water with increasing humidity, Phys. Chem. Chem. Phys. 1 (1999) 4619–4628. doi:10.1039/a904460d.

[85] I. Petrov, O. Shenderova, V. Grishko, V. Grichko, T. Tyler, G. Cunningham, G. Mcguire, Detonation nanodiamonds simultaneously purified and modified by gas treatment, Diam. Relat. Mater. 16 (2007) 2098–2103. doi:10.1016/j.diamond.2007.05.013.

[86] O. Shenderova, I. Petrov, J. Walsh, V. Grichko, V. Grishko, T. Tyler, G. Cunningham, Modification of detonation nanodiamonds by heat treatment in air, Diam. Relat. Mater. 15 (2006) 1799–1803. doi:10.1016/j.diamond.2006.08.032.

[87] V.L. Kuznetsov, M.N. Aleksandrov, I. V. Zagoruiko, A.L. Chuvilin, E.M. Moroz, V.N. Kolomiichuk, V.A. Likholobov, P.M. Brylyakov, G. V. Sakovitch, Study of ultradispersed diamond powders obtained using explosion energy, Carbon N. Y. 29 (1991) 665–668. doi:10.1016/0008-6223(91)90135-6.

[88] L. Schmidlin, V. Pichot, M. Comet, S. Josset, P. Rabu, D. Spitzer, Identification, quantification and modification of detonation nanodiamond functional groups, Diam. Relat. Mater. 22 (2012) 113–117. doi:10.1016/j.diamond.2011.12.009.

[89] O. Shenderova, A. Koscheev, N. Zaripov, I. Petrov, Y. Skryabin, P. Detkov, S. Turner, G. Van Tendeloo, Surface Chemistry and Properties of Ozone-Purified Detonation Nanodiamonds, J. Phys. Chem. C. 115 (2011) 9827–9837. doi:10.1021/jp1102466.

[90] J.R. Hardy, S.D. Smith, Two-phonon infra-red lattice absorption in diamond, Philos. Mag. 6 (1961) 1163–1172. doi:10.1080/14786436108239677.

[91] C.-L. Cheng, H.-C. Chang, J.-C. Lin, K.-J. Song, J.-K. Wang, Direct Observation of Hydrogen Etching Anisotropy on Diamond Single Crystal Surfaces, Phys. Rev. Lett. 78 (1997) 3713–3716. doi:10.1103/PhysRevLett.78.3713.

[92] C.-L. Cheng, J.-C. Lin, H.-C. Chang, The absolute absorption strength and vibrational coupling of CH stretching on diamond C(111), J. Chem. Phys. 106 (1998) 7411. doi:10.1063/1.473701.

[93] H. Mutschke, J. Dorschner, T. Henning, C. Jäger, U. Ott, Facts and Artifacts in Interstellar Diamond Spectra, Astrophys. J. 454 (1995) L157. doi:10.1086/309785.

[94] Y. Liu, Z. Gu, J.L. Margrave, V.N. Khabashesku, Functionalization of Nanoscale Diamond Powder: Fluoro-, Alkyl-, Amino-, and Amino Acid-Nanodiamond Derivatives, Chem. Mater. 16 (2004) 3924–3930. doi:10.1021/cm048875q.

[95] T. Petit, J.-C.C. Arnault, H.A. Girard, M. Sennour, T.-Y. Kang, C.-L. Cheng, P. Bergonzo, Oxygen hole doping of nanodiamond., Nanoscale. 4 (2012) 6792–9. doi:10.1039/c2nr31655b.

[96] M. V. Korobov, D.S. Volkov, N. V. Avramenko, L.A. Belyaeva, P.I. Semenyuk, M.A. Proskurnin, Improving the Dispersity of Detonation Nanodiamond: Differential Scanning Calorimetry as a new method of controling the aggregation state of nanodiamond powders., Nanoscale. 5 (2013) 1529–36. doi:10.1039/c2nr33512c.

[97] Y. Liu, V.N. Khabashesku, N.J. Halas, Fluorinated Nanodiamond as a Wet Chemistry Precursor for Diamond Coatings Covalently Bonded to Glass Surface, J. Am. Chem. Soc. 127 (2005) 3712–3713.

[98] N.O. Mchedlov-Petrossyan, N.N. Kamneva, A.I. Marynin, A.P. Kryshtal, E. Ōsawa, Colloidal properties and behaviors of 3 nm primary particles of detonation nanodiamonds in aqueous media., Phys. Chem. Chem. Phys. 17 (2015) 16186–203. doi:10.1039/c5cp01405k.

[99] T. Anzai, H. Maeoka, A. Wada, K. Domen, C. Hirose, T. Ando, Y. Sato, Vibrational sum-frequency generation spectroscopy of a homoepitaxially-grown diamond C(100) surface, J. Mol. Struct. 352–353 (1995) 455–463. doi:10.1016/0022-2860(94)08518-M.

[100] K. Xu, Q. Xue, A new method for deaggregation of nanodiamond from explosive detonation: Graphitization-oxidation method, Phys. Solid State. 46 (2004) 649–650. doi:10.1134/1.1711442.

[101] G. Cunningham, A.M. Panich, a I. Shames, I. Petrov, O. Shenderova, Ozone-modified detonation nanodiamonds, Diam. Relat. Mater. 17 (2008) 650–654. doi:10.1016/j.diamond.2007.10.036.

[102] T. Petit, J.-C. Arnault, H.A. Girard, M. Sennour, P. Bergonzo, Early stages of surface graphitization on nanodiamond probed by x-ray photoelectron spectroscopy, Phys. Rev. B. 84 (2011) 233407.

[103] J.-B. Brubach, A. Mermet, A. Filabozzi, A. Gerschel, P. Roy, Signatures of the hydrogen bonding in the infrared bands of water., J. Chem. Phys. 122 (2005) 184509. doi:10.1063/1.1894929.

[104] D.B. Asay, S.H. Kim, Evolution of the adsorbed water layer structure on silicon oxide at room temperature., J. Phys. Chem. B. 109 (2005) 16760–3. doi:10.1021/jp053042o.

[105] A. Anderson, W.R. Ashurst, Interfacial water structure on a highly hydroxylated silica film., Langmuir. 25 (2009) 11549–54. doi:10.1021/la901459b.

[106] S. Stehlik, M. Varga, P. Stenclova, L. Ondic, M. Ledinsky, J. Pangrac, O. Vanek, J. Lipov, A. Kromka, B. Rezek, Ultrathin Nanocrystalline Diamond Films with Silicon Vacancy Color Centers via Seeding by 2 nm Detonation Nanodiamonds, ACS Appl. Mater. Interfaces. 9 (2017) 38842–38853. doi:10.1021/acsami.7b14436.

[107] T.S. Varley, M. Hirani, G. Harrison, K.B. Holt, Nanodiamond surface redox chemistry: influence of physicochemical properties on catalytic processes, Faraday Discuss. 172 (2014) 349–364. doi:10.1039/C4FD00041B.

[108] L. Zhang, R.J. Hamers, Photocatalytic reduction of CO2 to CO by diamond nanoparticles, Diam. Relat. Mater. 78 (2017) 24–30. doi:https://doi.org/10.1016/j.diamond.2017.07.005.

[109] P. Hollins, Infrared Reflection–Absorption Spectroscopy, Encycl. Anal. Chem. (2006) 1–17. doi:10.1002/9780470027318.a5605.

[110] R.C. Alkire, D.M. Kolb, J. Lipkowski, P.N. Ross, eds., Advances in Electrochemical Science and Engineering, Wiley-VCH Verlag GmbH, Weinheim, Germany, 2006. doi:10.1002/9783527616817.

[111] B.L. Frey, R.M. Corn, S.C. Weibel, Polarization-Modulation Approaches to Reflection-Absorption Spectroscopy, Handb. Vib. Spectrosc. 2 (2001) 1042–1056. doi:10.1002/0470027320.s2206.

[112] J. Srajer, A. Schwaighofer, G. Ramer, S. Rotter, B. Guenay, A. Kriegner, W. Knoll, B. Lendl, C. Nowak, Double-layered nanoparticle stacks for surface enhanced infrared absorption spectroscopy, Nanoscale. 6 (2014) 127–131. doi:10.1039/C3NR04726A.

[113] K.L.A. Chan, L. Govada, R.M. Bill, N.E. Chayen, S.G. Kazarian, Attenuated total reflection-FT-IR spectroscopic imaging of protein crystallization, Anal. Chem. 81 (2009) 3769–3775. doi:10.1021/ac900455y.

[114] A. Greenaway, B. Gonzalez-Santiago, P.M. Donaldson, M.D. Frogley, G. Cinque, J. Sotelo, S. Moggach, E. Shiko, S. Brandani, R.F. Howe, P. a. Wright, In situ synchrotron IR microspectroscopy of CO2 adsorption on single crystals of the functionalized MOF Sc2(BDC-NH2)3, Angew. Chemie - Int. Ed. 53 (2014) 13483–13487. doi:10.1002/anie.201408369.

[115] M.C. Martin, U. Schade, P. Lerch, P. Dumas, Recent applications and current trends in analytical chemistry using synchrotron-based Fourier-transform infrared microspectroscopy,

TrAC - Trends Anal. Chem. 29 (2010) 453–463. doi:10.1016/j.trac.2010.03.002.

[116] M.J. Tobin, L. Puskar, R.L. Barber, E.C. Harvey, P. Heraud, B.R. Wood, K.R. Bambery, C.T. Dillon, K.L. Munro, FTIR spectroscopy of single live cells in aqueous media by synchrotron IR microscopy using microfabricated sample holders, Vib. Spectrosc. 53 (2010) 34–38. doi:10.1016/j.vibspec.2010.02.005.

[117] X.G. Xu, M. Rang, I.M. Craig, M.B. Raschke, Pushing the sample-size limit of infrared vibrational nanospectroscopy: From monolayer toward single molecule sensitivity, J. Phys. Chem. Lett. 3 (2012) 1836–1841. doi:10.1021/jz300463d.

[118] A. Cvitkovic, N. Ocelic, J. Aizpurua, R. Guckenberger, R. Hillenbrand, Infrared imaging of single nanoparticles via strong field enhancement in a scanning nanogap, Phys. Rev. Lett. 97 (2006) 1–4. doi:10.1103/PhysRevLett.97.060801.

[119] A. Dazzi, C.B. Prater, Q. Hu, D.B. Chase, J.F. Rabolt, C. Marcott, AFM – IR : Combining Atomic Force Microscopy and Infrared Spectroscopy for Nanoscale Chemical Characterization, Appl. Spectrosc. 66 N62 (2012) 1365–1384. doi:10.1366/12-06804.

[120] C. Marcott, T. Awatani, J. Ye, D. Gerrard, M. Lo, K. Kjoller, Review of nanoscale infrared spectroscopy applications to energy related materials, Spectrosc. Eur. 26 (2014) 19–23.

[121] F. Huth, A. Govyadinov, S. Amarie, W. Nuansing, F. Keilmann, R. Hillenbrand, Nano-FTIR absorption spectroscopy of molecular fingerprints at 20 nm spatial resolution, Nano Lett. 12 (2012) 3973–3978. doi:10.1021/nl301159v.

[122] H.A. Bechtel, E.A. Muller, R.L. Olmon, M.C. Martin, M.B. Raschke, Ultrabroadband infrared nanospectroscopic imaging, Proc. Natl. Acad. Sci. U. S. A. 111 (2014) 7191–6. doi:10.1073/pnas.1400502111.

[123] P.M. Donaldson, C.S. Kelley, M.D. Frogley, J. Filik, K. Wehbe, G. Cinque, Broadband near-field infrared spectromicroscopy using photothermal probes and synchrotron radiation, Opt. Express. 24 (2016) 1852–1864. doi:10.1364/OE.24.001852.

[124] D. Khanal, A. Kondyurin, H. Hau, J.C. Knowles, O. Levinson, I. Ramzan, D. Fu, C. Marcott, W. Chrzanowski, Biospectroscopy of Nanodiamond-Induced Alterations in Conformation of Intra- and Extracellular Proteins: A Nanoscale IR Study, Anal. Chem. 88 (2016) 7530–7538. doi:10.1021/acs.analchem.6b00665.

[125] I. Amenabar, S. Poly, W. Nuansing, E.H. Hubrich, A. a Govyadinov, F. Huth, R. Krutokhvostov, L. Zhang, M. Knez, J. Heberle, A.M. Bittner, R. Hillenbrand, Structural analysis and mapping of individual protein complexes by infrared nanospectroscopy., Nat. Commun. 4 (2013) 2890. doi:10.1038/ncomms3890.

[126] M.J. Baker, J. Trevisan, P. Bassan, R. Bhargava, H.J. Butler, K.M. Dorling, P.R. Fielden, S.W. Fogarty, N.J. Fullwood, K.A. Heys, C. Hughes, P. Lasch, P.L. Martin-Hirsch, B. Obinaju, G.D. Sockalingum, J. Sulé-Suso, R.J. Strong, M.J. Walsh, B.R. Wood, P. Gardner, F.L. Martin, Using Fourier transform IR spectroscopy to analyze biological materials, Nat. Protoc. 9 (2014) 1771–1791. doi:10.1038/nprot.2014.110.

[127] M. Miljković, B. Bird, M. Diem, Line shape distortion effects in infrared spectroscopy., Analyst. 137 (2012) 3954–64. doi:10.1039/c2an35582e.

[128] I. Noda, Two-dimensional infrared (2D IR) spectroscopy. Theory and applications, Appl. Spectrosc. 44 (1990) 550–561. doi:10.1366/0003702904087398.

[129] L. Puskar, E. Ritter, U. Schade, M. Yandrasits, S.J. Hamrock, M. Schaberg, E.F. Aziz, Infrared dynamics study of thermally treated perfluoroimide acid proton exchange membranes, Phys. Chem. Chem. Phys. 19 (2017) 626–635. doi:10.1039/C6CP06627E.

[130] C. Baudot, C.M. Tan, J.C. Kong, FTIR spectroscopy as a tool for nano-material characterization, Infrared Phys. Technol. 53 (2010) 434–438. doi:10.1016/j.infrared.2010.09.002.

[131] M. Mermoux, S. Chang, H.A. Girard, J.-C. Arnault, Raman spectroscopy study of detonation nanodiamond, Diam. Relat. Mater. 87 (2018) 248–260. doi:10.1016/J.DIAMOND.2018.06.001.

[132] J.C. Arnault, X-ray Photoemission Spectroscopy applied to nanodiamonds: From surface chemistry to in situ reactivity, Diam. Relat. Mater. 84 (2018) 157–168. doi:10.1016/J.DIAMOND.2018.03.015.